European Commission

JRC TECHNICAL REPORTS

Modelling inclusion, testing and benchmarking of the impacts of ozone pollution on crop yields at regional level

Module development and testing and benchmarking with the WOFOST generic crop model

Giovanni Cappelli
Roberto Confalonieri
Maurits Van Den Berg
Frank Dentener

UNIVERSITÀ DEGLI STUDI DI MILANO

Courtesy: Gina Mills, CEH, UK

Joint Research Centre

EUR 28395 EN

This publication is a Technical report by the Joint Research Centre (JRC), the European Commission's science and knowledge service. It aims to provide evidence-based scientific support to the European policy-making process. The scientific output expressed does not imply a policy position of the European Commission. Neither the European Commission nor any person acting on behalf of the Commission is responsible for the use which might be made of this publication.

Contact information

Name: Frank Dentener
Address: European Commission, Joint Research Centre, Directorate for Sustainable Resources, Via Enrico Fermi 2749, 21027 Ispra (VA), Italy
Email: frank.dentener@jrc.ec.europa.eu
Tel.: +39 0332 78 6392

JRC Science Hub
https://ec.europa.eu/jrc

JRC103907

EUR 28395 EN

PDF ISBN 978-92-79-64945-5 ISSN 1831-9424 doi:10.2788/68501

Luxembourg: Publications Office of the European Union, 2016

How to cite this report: G. Cappelli, R. Confalonieri, M. Van Den Berg, F. Dentener; *Modelling inclusion, testing and benchmarking of the impacts of ozone pollution on crop yields at regional level*; EUR 28395 EN, Luxembourg: Publications Office of the European Union, 2016, doi:10.2788/68501

Table of contents

Abstract

The WOFOST crop model -as implemented in the BioMA modelling framework- was extended with algorithms to account for the effects of ground-level ozone on crop growth and yield.

The additional algorithms implemented concern:

- Effect of water stress on stomatal conductance
- Reduction of carboxylation rate of Rubisco
- Ability of plants to partly recover from ozone damage
- Acceleration of leaf senesce due to O_3 exposure

Meteorological datasets, with a consistent hourly-daily temporal resolution, were selected for two locations in Germany (Bremen) and Spain (Jerez), encompassing different climatic conditions. The sensitivity of two types of crops was assessed: wheat, which is relatively sensitive to O_3 damage, and barley, which is less sensitive. These two crops were exposed to a range of hypothetical O_3 mixing ratios of 20, 40, and 60 ppb during the entire crop growth cycle, as well as during specific months. Two agro-managements options were analysed: a potential yield case (i.e. no water stress by mimicking a full crop irrigation case), and a rain-fed case. Irrespective of ozone, rainfed wheat and barley yields are lower by only 12 % in Bremen compared to fully irrigated crops, while strongly reduced by 55 % in Jerez. Additionally, wheat yield losses, up to 30 % are calculated for ozone concentrations of 60 ppb, and only half of these for barley. Yield losses are substantially smaller in Jerez for rain-fed crops, when stomatal closure is limiting gas exchange, and thus impeding photosynthesis, crop growth and yields, but also reducing ozone uptake.

General findings are:

- Crop damages due to O_3 exposure increase with O_3 concentration
- Effects of high O_3 concentrations are very heterogeneous depending on month, site, crop and the simulated variable considered
- The highest impact is obtained when the month with high O_3 concentration coincides with the anthesis/grain *filling* stage (June for Bremen, April for Jerez)
- Rain-fed crop damage is more marked in Bremen than Jerez and irrigation practice exacerbates O_3 damages, especially in Jerez
- Barley is less affected by O_3 impact according to the lower sensitivity of the crop.

The algorithms developed can easily be implemented in other (generic or crop-specific) models of similar complexity.

Compare model results against field data under diverse conditions will be the next phase of this work, and further model developments are needed to simulate so-called “stomatal sluggishness” (i.e. damage to the stomata due to ozone).

1. Introduction

Tropospheric ozone is a photochemically produced secondary pollutant whose precursors are nitrogen oxides (NO_x), methane and other volatile organic compounds and carbon monoxide. There is a wealth of evidence that at ground level, ozone is phytotoxic to plants, and can cause substantial damage to crops [Mills et al., 2007; Ainsworth et al, 2012]. Empirical evidence and model-based assessments suggest a large impact on crop yields globally, yet with marked variations across regions and with intricate interactions with climate change impact, adaptation and mitigation actions [Van Dingenen, et al., 2009; Burney and Ramanatan, 2014; Tai et al, 2014]. Ozone concentrations are already high in important crop-land areas in North America, Europe, and South and East Asia. Concentrations are increasing rapidly in developing countries and are projected to continue to increase in coming decades. However, the effects of ozone pollution are currently not considered in most crop models, including the WOFOST model, currently implemented in the BioMA framework, and used in the JRC MARS crop forecasting activity. Consequently, ozone effects are excluded from model predictions of regional crop growth and yield. A particular gap in our understanding is how ozone interacts with other stresses that effect crop growth, such as soil fertility, CO_2 fertilization, soil water stress, heat stress and even pests and diseases (e.g. ozone has been shown to make crops more vulnerable to attack by pests such as red spider mite). Nevertheless, there is sufficient information on the effect of ozone on crop physiology, particularly how it influences photosynthesis, C allocation and early senescence to warrant the development of ozone modules that could be embedded within existing crop models.

Based on the results of an expert contract with (Confalonieri, 2016) during the first semester of 2016, this report describes the work of experts from the University of Milano in collaboration with JRC, to include ozone in the BioMA modelling framework, to integrate it with the WOFOST model and to provide detailed meteorological datasets for testing the models.

The report is structured as follows:
Section 2 describes which version of the WOFOST model was used for this study and for which reasons; and which interaction mechanisms between ozone and plant growth were included in the ozone module.
Section 3 describes the test conditions that were designed to evaluate the sensitivity of the extended model.
Section 4 describes the new ozone effect algorithms implement in the
Section 5 describes the results of the preliminary modelling experiments that were conducted for the test conditions described in section 3.
Section 6 present recommendations and conclusions of the study.

2. Selection of WOFOST version and interaction mechanisms to study ozone effects on crops

Extensive experimental studies highlight the deleterious effects of chronic O_3 exposure on crop yields (Ainsworth et al., 2012). In such conditions, crop productivity is affected by a decreased CO_2 assimilation at leaf level (Amax; e.g. Feng et al., 2008) and a decreased synthesis of non-structural carbohydrates (i.e. sucrose, starch and pectins). These impacts on primary metabolism are partly responsible for the reduction of leaf area, a common response of field crops to O_3 enriched air (e.g., Morgan et al., 2004; Pang et al., 2009). In addition to lower carbon fixation, plants exposed to O_3 often display i) higher respiration rates (e.g., Amthor, 1988; Biswas et al., 2008), ii) altered biomass partitioning with decreased root biomass and redistribution of photosynthates from non-reproductive plant organs to grains and iii) a reduced leaf lifespan triggered by the acceleration of leaf senescence. All these responses contribute to the overall decrease in growth and yield. Interestingly, most of the processes affected are explicitly simulated by the WOFOST model (Diepen et al., 1989), which thus provides a suitable framework to integrate available models accounting for O_3 limitations within a crop growth model. Currently, two versions of WOFOST are implemented in BioMA (Stella et al., 2014; de Wit, 2014). They differ in the way by which they define the dependence of crop parameter values on air temperature and phenological development. The original WOFOST adopts so-called AFGEN tables to allow users to define arbitrary functions, which linearly interpolate between values of a dependent variable, Y, given a value of an independent variable, X, and a table of X and Y data pairs. In the new WOFOST-GT, such relations are described by simple mathematical equations, thus reducing model complexity and the number of parameters. Even though the second approach is deemed more elegant and sounder (since it reduces parameterization effort and the risk to fit unrealistic functions), we opted for using the original WOFOST which provides more flexibility and for which parameter sets are available which are widely used, including in the JRC MARS crop forecasting system. WOFOST is a generic crop simulator for annual field crops, based on a hierarchical distinction between potential and water-limited production. It performs its calculations with a one-day time step, using Euler integration to calculate the values of its state variables at the end of each day. Crop development rate is simulated as a simple function of temperature, photoperiod or both thermal and photoperiodic conditions. Photosynthesis (gross CO_2 assimilation) is simulated on the basis of intercepted photo-synthetically active radiation (PAR). Fluxes of direct and diffuse PAR are computed using Lambert-Beers law to estimate the light distribution in the canopy. The extinction coefficient for solar radiation can be customized according to the canopy architecture of the simulated crop. Maintenance respiration is assumed to be proportional to the dry weight of the plants organs, considering that different organs have different respiration/weight ratios depending on their composition. Assimilated carbon is partitioned among the different crop organs according to partitioning coefficients, modulated according phenological development. In this process, losses associated with conversion and growth respiration are accounted for. The daily increase in total LAI is estimated using a two-stage approach: using an exponential function driven by temperature during early growth phases, and from specific leaf area (SLA) and daily increase in leaf dry weight later on. LAI is then distributed within the canopy according to Gaussian Integration distances. Non-photosynthesis (dead) LAI units are computed daily

as a function of self-shading and senescence. A diagram showing the main processes accounted for by the WOFOST model and the possible coupling points to an idealised model reproducing the effects of O_3 on plant growth is shown in Figure 1.

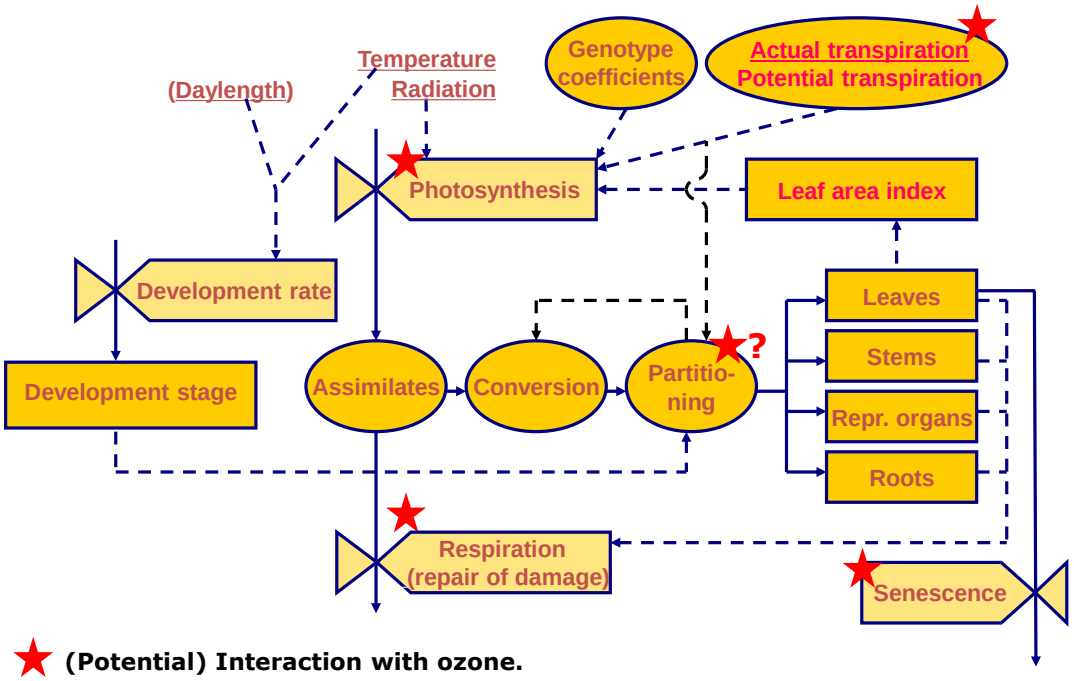

Figure 1. Flow chart of the processes implemented in the WOFOST model. Red stars indicate the processes that are subjected to ozone effects

Some adaptation to the model is required to enable consistent estimates of O_3 damages. In the BioMA framework, this is done within the so-called AbioticDamage component. An overview of adaptations considered is given in Table 1.

First, it is important to note that O_3 damage largely depends on the flux of the gas into plant tissues, which, in turn, is largely controlled by stomatal aperture. This means that either WOFOST or the O_3 impact models that will be plugged into the modelling solution have to calculate stomatal conductance (transpiration is using Penman- CO_2 fluxes $=H_2O$ flux). Although different models are available in literature (e.g. Leuning 1995; Medrano et al., 2002; Tuzet et al., 2003), the approach used by AquaCrop (Raes et al., 2009) seems to represent the best trade-off among the i) compatibility with the level of detail used by WOFOST to represent crop processes, ii) availability of input data usually stored in agrometeorological databases, iii) the availability of sets of proved parameters to differentiate crop-specific responses to water stress.

Moreover, even though WOFOST currently updates state variables with a daily time step, it could be important to estimate the O_3 movement into the mesophyll (controlled by stomata) at a shorter integration time step. The calculation of hourly fluxes could be a viable solution. The main reason for this is related to the diurnal variation of both O_3 tropospheric concentration – rising with high sunlight and temperature – and stomatal conductance, which are often coupled and sometimes decoupled (e.g., when excess light and temperature cause at the same time depression of photosynthesis and high O_3 concentrations). This could be managed by calculating, for all the groups of emitted GAI (green leave area index) units

having the same age, O_3 fluxes at hourly time step in the range of the daylight hours and then averaging the sum of hourly fluxes on the total number of contemporaneous age classes in the day. Daily averaged fluxes were then used to compute the O_3-induced fractional reduction of daily photosynthesis rates as simulated by WOFOST model. Another solution could be to convert WOFOST to hourly time step for all assimilation processes; which however was not yet possible with the time and resources allocated for this project. A case study comparing methods should be considered.

While O_3 uptake depends on stomatal conductance, it is also known that O_3 can affect stomatal conductance. This can be a reducing effect (Morgan et al., 2003), probably because of the reduced photosynthesis and the related increase of CO_2 concentration in the mesophyll, or because of the formation of plant hormones in response to ozone, such as ethylene, which induces stomatal closure. Another key aspect in modulating stomatal conductance and O_3 damages is water uptake: different experiments corroborate the hypothesis that drought mitigates the impact of O_3 by causing stomatal closure, thus reducing O_3 flux into leaves. On the other hand, Wilkinson and Davies (2009) highlight an increasing effect, attributed to the loss of functionality of stomata in O_3-stressed plants, which remain open despite drought stress. This phenomenon, often referred to as ozone-induced stomatal sluggishness, has the potential to sensibly change the carbon and water balance of crops (Paoletti and Grulke 2005). Several approaches were inspected to understand their potential impact, were they to me implemented in the ozone model. The approach of Hoshika et al. (2015) (see table 1) appears to be promising but would require validation for its applicability to annual crops prior to its implementation.

Ozone is usually detoxified in plants at uptake rates below a critical threshold, above which the rate of photosynthesis decreases. The ability of crops to resist to low ozone concentrations via detoxification and repair is strictly dependent on leaf age (Alsher and Amthor 1988), with young leaves being able to tolerate higher O_3 concentrations and completely repair from damage in a relatively short time (from hours to days) depending on the cultivar and pedoclimatic conditions (Pell et al., 1997). Nevertheless, prolonged exposure to even low O_3 concentrations is responsible for enhancing rates of leaf senescence, thus reducing the period during which plants can recover from ozone damage.

In any case, reliable estimates of drought stress and its impact on stomatal conductance requires the simple single-layer soil-water-plant-uptake approach of the WOFOST model to be replaced by a more elaborated soil water redistribution and uptake model; for example those implemented within the software component UNIMI.SoilW. For this study we decided to adopt:

- A multi-layer cascading approach (Ritchie, 1998) to simulate the downward movement of water through the soil profile: water fills up the layers until field capacity is reached, with the fraction exceeding this threshold moving to the deeper layer.
- The EPIC (Williams et al., 1989) approach to calculate root water uptake from each layer, requiring rooting depth, soil water content and crop potential transpiration as input variables.

These approaches appear suitable for the purpose of this study, since their limited input requirements are consistent with data availability over large scales.

Table 1. Inspected biophysical processes, model approaches and modifications needed to couple the original approaches to the BioMA AbioticDamage O_3 model. I: implemented; NI: not implemented.

Biophysical process	Model approaches and modifications	Action
1.2.1.1.1.1.1 Effect of water stress on stomatal conductance	1.2.1.1.1.1.2 A water stress related factor that multiplies the stomatal conductance (0 =maximum reduction; 1 = no effect) is introduced in the algorithm computing O_3 fluxes already implemented in the original O_3 model available in the AbioticDamage component. following the approach used by AquaCrop (Raes et al., 2009).	1.2.1.1.1.1.3
Reduction of carboxylation rate of rubisco	According to Ewert and Porter (2000). Decreases in rubisco-limited rate, distinguish between i) immediate effects due to high ozone fluxes and ii) long terms effects driven by leaf senescence acceleration. Since decreases in daily rate of gross photosynthesis are implicitly induced by the reduction in GAIs associated to the faster ageing of each contemporaneous class of GAI units, the average long-term reducing factor will not be applied to further reduce the actual daily gross CH_2O assimilation rate calculated by WOFOST. The rationale for this is to reduce the risk of markedly overestimating the effect of senescence on reducing photosynthesis rates, double counting its impact on plant growth.	1.2.1.1.1.1.4
1.2.1.1.1.1.5 Ability of plants to recover from ozone damage	According to Ewert and Porter (2000), the recovery from ozone-induced damage in a given day is used to modulate the ozone impact on rubisco-limited rate of photosynthesis at light saturated conditions of the following day, depending on leaf age. Since WOFOST considers LAI emitted units, instead of individual leaves, recovery factors are computed each day for all LAI units with the same age.	I
Metabolic cost (Increased respiration) to avoid or repair ozone damage		NI

1.2.1.1.1.1.6 Acceleration of leaf senescence due to O_3 exposure	1.2.1.1.1.1.7 Enhanced rates of senescence induced by prolonged exposure to O_3 in a given day is computed daily for each GAI unit of the same age class using reducing factors (0 = maximum reduction; 1 = no effect; unit less) calculated as function of cumulative ozone uptake (Ewert and Porter, 2000). An average indicator targeting the shortening of leaves lifespan due to ozone exposure is computed by averaging the sum of all daily factors on the total number of contemporaneous GAI age classes.	1.2.1.1.1.1.8
1.2.1.1.1.1.9 Reduction of green leaf area index due to foliar chlorosis or necrosis induced by O_3	1.2.1.1.1.1.10 An extensive literature search needs to be carried out to find out approaches that are i) coherent (neither too rough nor too refined) with the level of detail used by WOFOST and O_3 models and ii) use standard input variables. As an alternative, if measured data are available from literature, one could derive generic response functions triggered by a crop–specific sensitivity parameter set to 0 (or to 1) in case of no impact.	1.2.1.1.1.1.11
1.2.1.1.1.1.12 Stomatal sluggishness	1.2.1.1.1.1.13 The approach from Hoshika et al. (2015) accounts for the effect of chronic exposure to ozone on stomatal sluggishness by progressively increasing the minimum crop-specific stomatal conductance via a sigmoid function having the cumulative ozone uptake as independent variable. This model, as is, cannot be coupled directly with the AbioticDamage ozone model; but its implementation could be considered to modulate for instance the instantaneous O_3 leaf uptake over a plant-specific threshold ($UO_{>FO3crit)}$ according to the following equation: $UO_{Slug} = UO_{>FO3crit} \cdot \frac{g_{min\,S}}{g_{min}}$ $UO_{Slug} = UO_{>FO3crit} \cdot \frac{g_{min\,S}}{g_{min}}$ 1.2.1.1.1.1.14 Where: g_{min} (mol m^{-2} s^{-1}) is the minimum stomatal conductance in the	1.2.1.1.1.1.16

	absence of O_3; g_{minS} (mol m^{-2} s^{-1}) is the minimum stomatal conductance accounting for stomatal sluggishness as computed by Hoshika et al. (2015). 1.2.1.1.1.1.15 A strong limitation of Hoshika's approach is an empirical relationship developed for temperate deciduous forests and thus needs to be validated against measured data on herbaceous crops before being used outside the conditions for which it was calibrated.	

3. Test conditions to evaluate the sensitivity of the modelling solution to ozone exposure

A set of synthetic test conditions was generated to assess the crop model response in a range of environmental conditions for different crops, to verify model behaviour and to allow intercomparison with other models.

A first set of simulations was set up for two winter cereals with distinct tolerance to O_3 and environmental characteristics (such as different O_3 atmospheric concentrations). The two crops considered markedly differ in the sensitivity to ozone damage - i.e. winter wheat (susceptible) and winter barley (tolerant) – but share many phenological and productive traits[1]. This approach will greatly facilitate the analysis of results, allowing to separate the effects of O_3 exposure on crops from any possible interference due to interspecific differences in crop development and growth. Simulations were performed for two locations: 1) Bremen, in northwestern Germany, with a marine temperate humid climate and high yield potential, and 2) Jerez de la Frontera, Spain with Mediterranean climate with average-low yield potential. For each region, 20-years time series of meteorological data were selected [Table 4] to run simulations under rain-fed as well as under fully irrigated conditions. In this way, the potential interaction of ozone with drought conditions is explored (e.g., Morgan et al., 2003; Feng et al., 2008). Furthermore, such sample size is deemed large enough to capture the short-term random fluctuations – such as daily weather variations –, seasonal and interannual variability, as well as most part of the less frequent climate events that may occur in a given agro-ecosystem (Semenov and Barrow 2002). In this context simulations are performed by considering a sandy-loam soil, with a relatively low water holding capacity. Two reference levels of ozone concentrations are chosen: a sustained (without any daily or monthly variation) background ozone of 40 ppb and an elevated ozone of 60 ppb, respectively representative for background (inflow) O_3 and elevated continental O_3 concentrations (Feng and Kobayashi, 2009). As current model calibrations may implicitly include some effect of ozone in the parameterization, simulations were also performed using a pre-industrial ozone concentration – i.e. 20 ppb – as reference control, to test the model in presence of negligible ozone damages. For this first analysis synoptic and diurnal variations of ozone are ignored, as they may complicate the analysis. We note that this range also encompasses future (2030) annual ozone levels under a variety of scenarios for 2000-2030- with projected regional changes ranging from ca. -8 to +15 ppb - depending on scenario and region considered (Figure 2; Fiore et al., 2012; Kirtman et al., 2013).

[1] The same parameterization is operatively used for both crops within the JRC MARS crop growth monitoring system (CGMS)

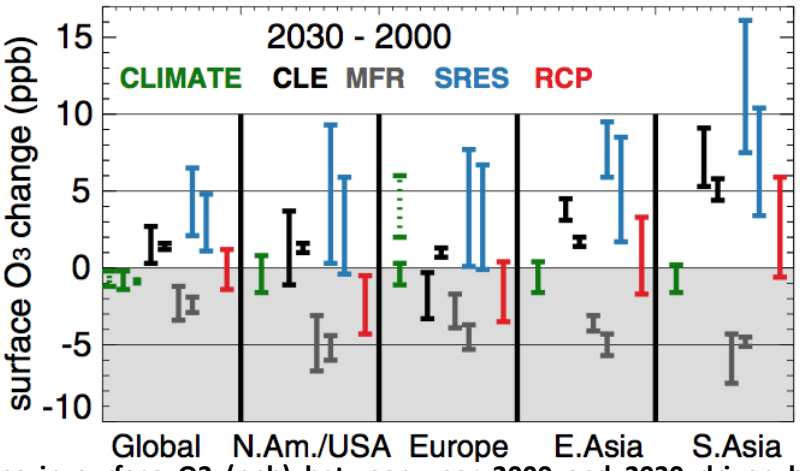

Figure 2. Changes in surface O3 (ppb) between year 2000 and 2030 driven by climate alone (CLIMATE, green) or driven by emissions alone, following current legislation (CLE, black), maximum feasible reductions (MFR, grey), SRES (blue) and RCP (red) emission scenarios. Results are reported globally. Where two vertical bars are shown (CLE, MFR, SRES), they represent the multimodel standard deviation of the annual mean based on the Atmospheric Composition Change: a European Network (ACCENT)/Photocomp study (Dentener et al., 2006) and (right bar) the parametric HTAP ensemble (Wild et al., 2012; four SRES and RCP scenarios included). Under Global, the leftmost (dashed green) vertical bar denotes the spatial range in climate-only changes from one model (Stevenson et al., 2005) while the green square shows global annual mean climate-only changes in another model (Unger et al., 2006). Under Europe, the dashed green bar denotes the range of climate-only changes in summer daily maximum O_3 in one model (Forkel and Knoche 2006). Source Kirtman et al., 2013 in IPCC-AR5 report.

In addition to examining the effects on crop growth and yield of constant ozone concentration throughout the growing season, we also tested the model response to monthly variations in O_3 concentration. For this purpose all months are set at the background ozone level (i.e. 40 ppb), except one, which is set at high ozone concentration (i.e. 60 ppb). Simulations are performed iteratively by changing each time the month displaying high O_3 concentrations, in order to identify the most critical phases of the crop cycle with regards to ozone exposure. The synopsis of the conditions explored is provided in Table 2; the total number of simulations (56) is determined by all the possible combinations of the factors and levels tested.

Table 2. Factors and levels tested in the first phase of the simulation experiment. Total number of simulation is 64.

Factor	Levels
Crop	Winter C3 (wheat, barley)
O_3 susceptibility	Tolerant (winter barley)
	Susceptible (winter wheat)
Climate	Marine
	Mediterranean
Precipitation	Rainfed
	Full irrigated
Soil texture	Medium/sandy-loam
O_3 concentration (ppb)	20 whole cycle
	40 whole cycle
	60 whole cycle
	60 February
	60 March
	60 April
	60 May
	60 June

For each combination of conditions tested, selected model output is stored (Table 4) to gain insight into the modelled effect of ozone damage on crop growth and productivity. In particular, daily values of aboveground biomass, green leaf area index and storage organs biomass are used as key variables influenced by photosynthesis activity. Variables related to water use, such as daily and cumulative evapotranspiration and water stress index (i.e., the ratio between potential and actual transpiration), are used to distinguish the impacts of losses due to water stress and stomatal closure from the losses due to ozone exposure. Final yield, harvest index and total water use are chosen as the synthetic variables describing crop productivity. Furthermore daily and cumulative O_3 fluxes to stomata and the percentage reduction of daily assimilation rates are tracked to separately inspect the effects of short- and long-term exposure to O_3. A summary of data needed as input for the modelling solution and simulated outputs is given in Tables 3 and 4.

Table 3. List of inputs needed to run the modelling solution under the test conditions defined in Table 1. Inputs are grouped in three classes, related to i) daily meteorological data, ii) crop management data and iii) Soil properties initialization data.

Inputs	Unit
Daily meteorological data	
Maximum air temperature	°C
Minimum air temperature	°C
Cumulative precipitation	mm
Average wind speed	mm s^{-1}
Minimum relative air humidity	%
Maximum relative air humidity	%
Global solar radiation	MJ m^{-2} d^{-1}
Reference evapotranspiration	mm
Latitude	°
Tropospheric Ozone concentration	ppb
Crop management data	
Sowing date	doy
Irrigation starting date	doy
Harvest date	doy
Soil properties initialization data	
Horizon thickness	m
Volumetric water content at saturation	m^3 m^{-3}
Volumetric wilting point	m^3 m^{-3}
Volumetric field capacity	m^3 m^{-3}
Saturated hydraulic conductivity	mm h^{-1}
Bulk density	t m^{-3}
Texture*	%
Number of layers	-
Layer thickness	m
Skeleton	%

* percentage of clay, silt and sand

Table 4. List of simulated outputs analyzed. Variables are grouped in three classes, related to i) water management, ii) crop productivity and iii) ozone damage to crop.

Simulated output	Unit
Water management	
Daily ET_0	mm d^{-1}
Cumulative ET_0	mm
Water stress index	-
Water stress effect on stomatal conductivity	-
Crop productivity	
Daily aboveground biomass	kg ha^{-1}
Daily green leaf area index	m^{-2} m^{-2}
Final yield	kg ha^{-1}
Harvest index	-
Cumulative water uptake	mm
Ozone damage	
Instantaneous O_3 fluxes to stomata	nmol m^{-2} s^{-1}
Cumulative O_3 fluxes to stomata	nmol m^{-2}
Percentage A_{max} reduction	%

ET_0: reference evapotranspiration; A_{max}: maximum leaf CO_2 assimilation rate (Kg ha^{-1} h^{-1}), WOFOST parameter.

In order to identify eligible test sites where to perform the first phase of simulation experiment, we crossed the information from the i) European climate classification according to the Köppen-Giger taxonomy (Figure 3; Peel et al., 2007), ii) maps of wheat and barley production area coverage and productivity by country (Figure 4; Bioma, 2016; FAOSTAT 2016), iii) the within country percentage cover occupied by selected species (USDA 2016), iv) the presence of reliable, consistent and accessible data sources, able to provide long time series of meteorological data, essential as input for the modelling solution.

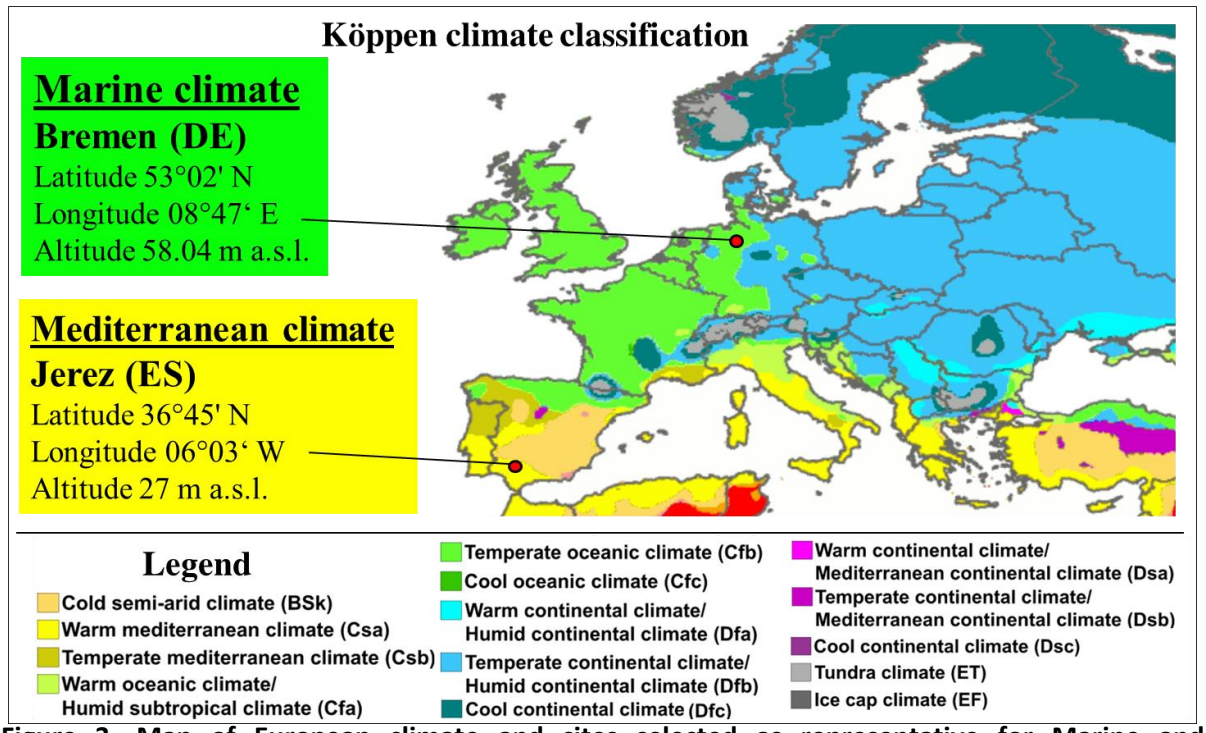

Figure 3. Map of European climate and sites selected as representative for Marine and Mediterranean climates.

As result, data from meteorological stations located close to Bremen, in northwestern Germany, and to Jerez de la Frontera, in south-western Spain, were selected as representative for Marine and warm Mediterranean climate. By analyzing data on the average production quantities by country available in the FAOSTAT database in the period 1993-2013, both countries prove to be among the top wheat and barley producers in the EU-27 (Figure 4).

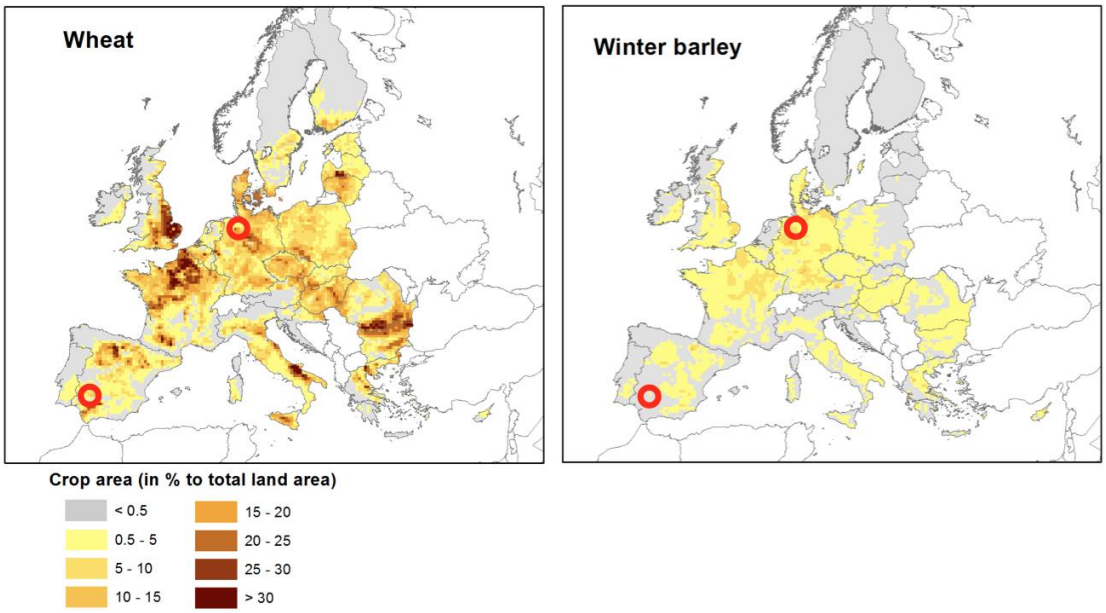

Figure 4. Crop area- production area for wheat and barley (http://bioma.jrc.ec.europa.eu). Red circles represent the sites selected to run the first set of simulations.

The economic importance of the two winter cereals in the target sites is confirmed by the high percentage of wheat and to a smaller extent barley harvested area in the region/state of belonging (Figure 4).

It can be noticed that the selected crops markedly differ in the average yields achieved, according to the crop suitability to pedo-climatic conditions in the target areas. While yields in Niersachsen, around Bremen, fluctuate around 7.5 t ha^{-1} (± 0.52 tha^{-1}) for wheat and 6.0 ha^{-1} (± 0.54 tha^{-1}) for barley, in Andalucia (Jerez de la Frontera) both crops show average yields of about 2.9 t ha^{-1} with a standard deviation ranging from 0.49 t ha^{-1} to 0.57 tha^{-1}.

For both sites, daily maximum and minimum air temperature (°C), precipitation (mm), average wind speed (m s^{-1}) and relative air humidity (%) were extracted from the European Climate Assessment & Dataset (ECA&D; http://eca.knmi.nl/). Global solar radiation (MJ m^{-2} d^{-1}) and reference evapotranspiration (ET_0; mm) were generated according to Hargreaves (Hargreaves and Samani 1982) and FAO (Allen et al., 1998) equations respectively. The monthly patterns of meteorological variables collected within the period 1996-2015 were then analyzed; some synthetic previews are shown in Appendix (Figure 1 and 2). In addition, the above listed daily data were used to generate hourly values of meteorological drivers, in order to produce an hourly meteorological dataset consistent with the daily one, to be used as input to the hourly time step O_3 models for future intercomparisons. To generate synthetic hourly data, the following approaches were adopted:

- hourly air temperature: Campbell (1985);
- hourly air relative humidity: Waichler and Wigmosta, 2003;
- hourly wind speed: Mitchell et al., 2000;
- hourly rainfall: Meteotest 2003;
- hourly radiation: Chen et al., 1999;
- hourly reference evapotranspiration: Allen et al., 1998.

An overview of weather variables patterns in both sites is given in Appendix A.

Options for future work:

Once results will be definitive, the reference simulation protocol could be reiterated on the same crops by changing soil texture and/or adopting more realistic patterns of monthly mean surface ozone concentrations (e.g., Avnery et al., 2011). As an alternative, the setup of simulation experiment could be applied to other C3 species or even to C4 summer crops (extending to September), which generally show a lower sensitivity of plant growth to O_3 concentrations than C3 species (Table 3; Sitch et al., 2005).

4. The modelling solution and modifications to the AbioticDamage component

4.1. The modelling solution

The third phase of the workflow dealt with the realization of a customized modelling solution for the simulation, with daily time step, of ozone (O_3) damages to crops The developed modelling solution links (i) the original WOFOST version implemented in the software component UNIMI.CropML, (ii) soil water redistribution and uptake models collected by UNIMI.SoilW and (iii) the amended ozone impact model present in UNIMI.AbioticDamage (Figure 5).

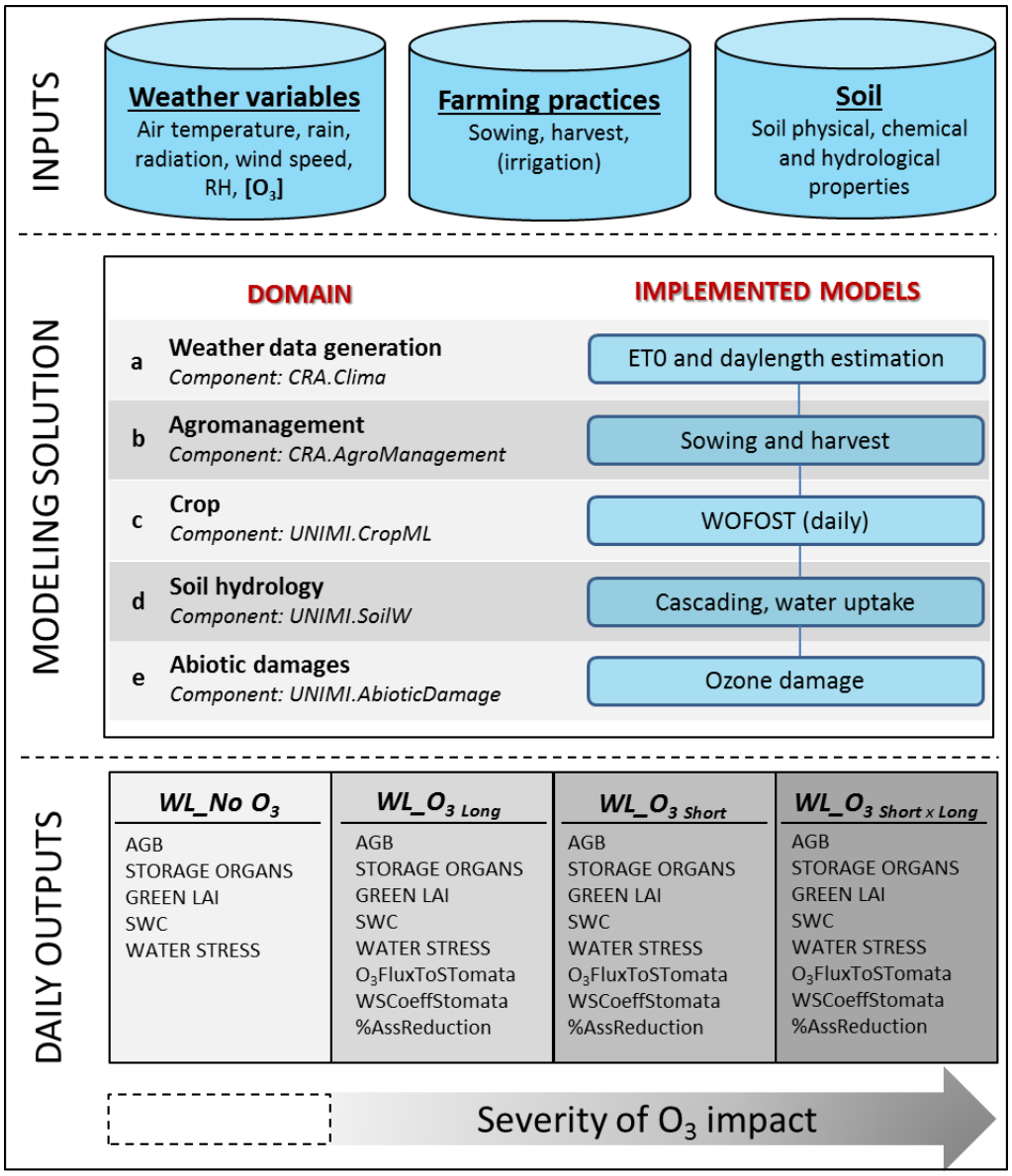

Figure 5. Schematic representation of the models composing the modelling solution and the components they belong to.

The CropML_SoilW_AbioticDamage_solution project handles the interactions between the I/O data produced by models belonging to the software components, in order to simulate the

different biophysical processes shown in Figure 5. The entry point of the modelling solution is the RunnerAPI class, containing instances of Adapter classes (Gamma et al., 1994) and managing their call. Adapter classes, in turns, encapsulate the logic to perform dynamic simulations, by calling specific models selected among those provided by software components. The components implemented in the modelling solution communicate in each integration time step (daily), via the methods provided by ISimulationComponent interface. Information produced during the simulation is stored in dedicated classes i.e., DataTypes, containing the instances of the data structures of the components implemented in the modelling solution. DataTypes are also used to store input data from different sources (e.g., meteorological data, pedological information). All DataTypes are shared by all the Adapter classes of the MS, making possible the communication of models belonging to different domains, meant as the possibility of exchanging variables among software components. The Adapter class of the component CRA.AgroManagement is able to publish specific events (e.g., planting, harvest), which are listened by other Adapters via the HandleEvents method of the ISimulationComponent interface.

4.2. Input data layers

The data needed as inputs to the CropML_SoilW_AbioticDamage_solution are organized in information layers and integrate data from different sources, allowing an ease coupling with biophysical models.

- **Weather** layer contains .txt files collecting daily meteorological data covering the whole simulation period for the site to be tested. Weather variables included in the sample weather file used to test the modelling solution are the following: daily minimum and maximum air temperatures (°C), rainfall (mm), average wind speed (m s^{-1}) global solar radiation (MJ m^{-2} d^{-1}) minimum and maximum relative humidity (%) and Ozone concentration (parts per billion, ppb).
- **Farming practices** layer is represented by a single .xml file which currently includes the crop species grown, the sowing and harvest date and the planting depth for each combination site × year. This layer can be modified and/or extended by the user by specifying different sets of rules and impacts to simulate alternate management strategies.
- **Soil** layer is made up by an .xml file collecting the parameters to set the physical and hydrological properties along the soil profile at the beginning of simulation. Main soil properties concern: horizon thickness (m), volumetric water content at saturation (m^3 m^{-3}), volumetric wilting point (m^3 m^{-3}), volumetric field capacity (m^3 m^{-3}), saturated hydraulic conductivity (mm h^{-1}), bulk density (t m^{-3}), texture (i.e. relative percentage of clay, silt and sand; %), skeleton (%), number of layers (unit less) and layer thickness (m).

4.3. The modelling layers within the modelling solution

Approaches implemented in each modelling layer are outlined in the following list:

a. **CRA.Clima** is used to estimate reference evapotranspiration according to the Hargreaves equation (Hargreaves and Samani, 1985), which requires daily minimum and maximum temperature and extra-terrestrial solar radiation as input. The latter is calculated by the component as an integration of hourly radiation estimated from the solar constant, zenith

angle and a correction parameter specific for each day of the year. Day length is estimated as function of latitude and solar declination.

b. **CRA.AgroManagement** triggers the occurrence of agricultural operations at run time according to (i) set of rules based on management decisions (e.g., scheduled events) and/or some states of the system. This components currently handles – within the solution – sowing and harvest operations, with the possibility of including dedicated rules to manage irrigation events according to the method (e.g. sprinkler, surface flow, drip or flood irrigation) and the scheduling time needed (i.e. turn or plant needs based irrigation). For instance, the fully irrigated treatment as defined in the test condition report (no stress due to water shortage), was reproduced here according to an automatic rule which triggers an irrigation event every time that the water stress index is lower than one, bringing the volumetric soil water content in the rooted soil back to field capacity.

c. **UNIMI.CropML** implements the model WOFOST. Crop development is simulated as a thermal-driven process. Instantaneous gross CO_2 assimilation is estimated in three moments during the day as a function of intercepted radiation and of a photosynthesis-light response curve of individual leaves. Light interception depends on total incoming radiation, on photosynthetic leaf area and on leaf angle distribution. Canopy architecture is divided into three horizontal layers with LAI split among them using Gaussian integration. Biomass partitioning is driven by partitioning factors and efficiencies of assimilates conversion into the different organs (i.e., growth respiration). Daily increase in total LAI is estimated as a function of temperature during early growth whereas it is derived from specific leaf area and development stage later on. Non-photosynthetically active (dead) LAI units are computed each day as a function of canopy self-shading and senescence. Potential evapotranspiration is estimated using the Penman approach (Frere and Popov, 1979), and water stress is derived by the actual to potential transpiration ratio.

d. **UNIMI.SoilW** is used to simulate soil water redistribution among soil layers according to a cascading (tipping bucket) approach. The changes of soil water content and fluxes among layers are provided as output; water percolating from the bottom layer is lost from the soil column. The component also estimates root water uptake based on evapotranspiration demand, soil water content and variable root depth. The component does not simulate water infiltration. Input water is assumed to be net rain able to infiltrate the soil. No attempt to compute runoff, plant and mulch interception is performed. The component also allows the simulation of effective plant transpiration, soil evaporation and the effects of soil tillage and subsequent settling of hydrological properties of the soil (field capacity, wilting point, retention functions, conductivity functions, bulk density). The latter are not taken into account in the current modelling solution.

e. **UNIMI.AbioticDamage** contains a complex model for the simulation of the crop damages due to ozone. It implements a model of leaf aerodynamic and boundary layer resistance (Spiker et al., 2007), the calculation of average leaf conductance proposed by Georgiadis et al. (2005), and the fractional reduction of plant production in function of the ozone flux through the stomata and the leaf conductance of water, according to the approach proposed by Sitch et al. (2005).

4.4. UNIMI.AbioticDamage modifications

As discussed in section 2 of this report (Selection of WOFOST version and interaction mechanisms to study ozone effects on crops), the O_3 model implemented in the UNIMI.AbioticDamage component has been modified to account for some O_3 effects on crop growth not considered in the original version.

4.4.1. Effect of water stress on stomatal conductance

A water stress related factor modulating the stomatal conductance (K_s, 0 =maximum reduction due to water stress-induced stomatal closure; 1 = no effect; unitless) was introduced in the algorithm computing the instantaneous O_3 leaf uptake over a critical threshold ($UO_{>FO3crit}$; Equation 1, Sitch et al., 2005) to adjust O_3 fluxes to stomata (FO_3, nmol m^{-2} s^{-1}).

$$UO_{>FO3crit} = \max\left[\left(FO_3 \cdot K_s - FO_{3crit}\right), 0\right] UO_{>FO3crit} = \max\left[\left(FO_3 \cdot K_s - FO_{3crit}\right), 0\right] \quad [1]$$

Where: FO_{3crit}, (nmol m^{-2} s^{-1}) is a plant-specific critical threshold below which the damage to tissues due to O_3 leaf uptake is equal to 0. In other words, the lower the threshold, the higher is the plant susceptibility to O_3 damage.

Ks response function is computed according to the approach used in the model AquaCrop (Equation 2; Figure 5; Raes et al., 2009).

$$K_s = \begin{cases} 1 & if \;\; Drel = 0 \\ 1 - \dfrac{e^{D_{rel} \cdot f_{shape}} - 1}{e^{f_{shape}} - 1} & if \;\; 0 < Drel < 1 \\ 0 & if \;\; Drel = 1 \end{cases} \quad [2]$$

Where: D_{rel} (%) is the fraction of water depleted in the root zone relative to the full amount the soil can hold between an upper (p_{upper}) and lower (p_{lower}) critical threshold of total available soil water (TAW); f_{shape} (unit less) is a crop specific parameter modulating the shape of the response curve (e.g. 2.5 for wheat, 6 for maize and sorghum, 3, for rice, potato and soybean, 2 for sunflower).

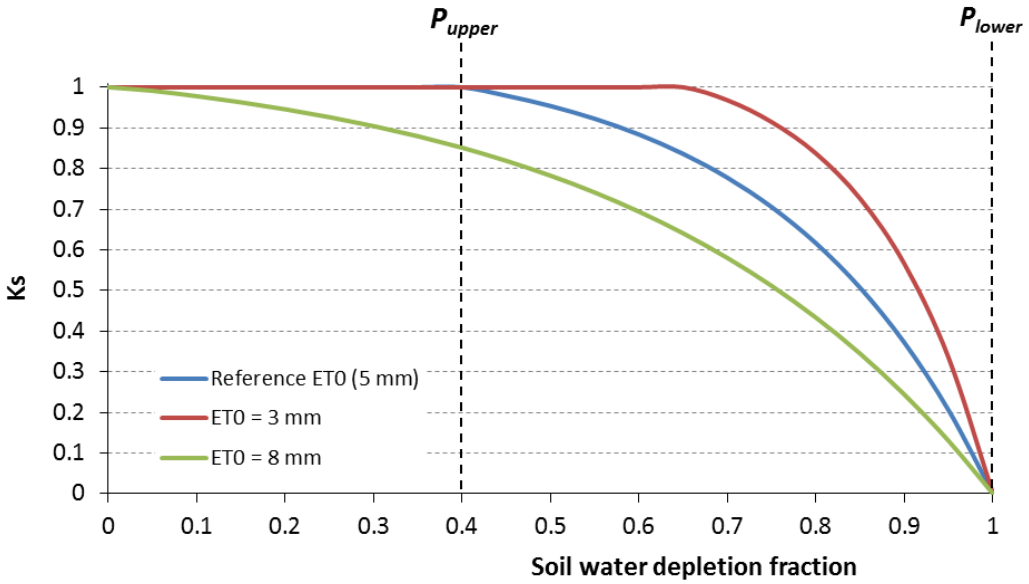

Figure 5. Stomatal conductance response function(ks, unitless) to relative depletion of soil water and evapotranspiration demand.

The critical thresholds are expressed as a fraction of TAW, with the lower one set to permanent wilting point (p_{lower}=1); D_{rel} is computed according to equation 3.

$$D_{rel} = \frac{\left(\frac{FC - WC}{FC - WP}\right) - p_{upper}}{1 - p_{upper}} \quad D_{rel} = \frac{\left(\frac{FC - WC}{FC - WP}\right) - p_{upper}}{1 - p_{upper}} \qquad [3]$$

Where: FC (m^3 m^{-3}) is the volumetric soil water content at field capacity; WC (m^3 m^{-3}) is the actual volumetric soil water content in the rooted zone; WP (m^3 m^{-3}) is the volumetric soil water content at wilting point.

Tabular values for the upper threshold (p) are given for different crops at a reference evaporative demand of ET_0 = 5 mm d^{-1}; for different levels of ET_0, p_{upper} is adjusted at runtime according to the equation 4 (Raes et al., 2009).

$$0 \le P_{upperadj} = p_{upper} + f_{adj}\left[0.04 \cdot (5 - ET_0)\right] \cdot \log_{10}\left(10 - 9 \cdot p_{upper}\right) \le 1 \qquad [4]$$

Where: f_{adj} (unit less, default value = 1) is a model parameter set to increase (>1) or decrease (<1) the p_{upper} adjustment.

The log term in the equation 4 amplifies the adjustment when the soil is wet compared to when it is dry, based on the likely restriction of stomata and transpiration (and thus a lower effect of the evaporative demand) when the soil is dry.

4.4.2. Reduction of daily rate of gross photosynthesis

The library of O_3 impact models on photosynthesis rates implemented in UNIMI.AbioticDamage component (Sitch et al., 2005) was extended by including the approach developed by Ewert and Porter (2000), which models the decreases in the hourly rates of net photosynthesis distinguishing between (i) immediate effects due to high ozone fluxes and (ii) long term effects driven by leaf senescence acceleration. In order to allow the new ozone impact model based on thea SUCROS approach of photosynthesis (Van Ittersum et al., 2003), originally developed for Farquhar (Farquhar et al., 1980),) we applied the ozone damage factors to reduce the actual daily gross CH_2O assimilation rate, as driven by the maximum leaf CO_2 assimilation rate (A_{max}, Kg ha^{-1} h^{-1}) limited by temperature and solar radiation absorbed by the shaded and sunlit leaves. Since the WOFOST model considers the Green Area Index (GAI) emitted units, instead of leaves surface, both short- and long-term effects are computed each day for all the groups of emitted GAI units having the same age and then averaging the sum on the total number of contemporaneous age classes.

4.4.2.1. Short-term response and ability of plant to recover from ozone damage

The short-term O_3 effect on photosynthesis is computed daily for all GAI units of the same age class using a short-term hourly damage factor ($GAI\_fO_{3,s(h)}$, 0 = maximum reduction; 1 = no effect; unit less) calculated, for each daylight hour, using a linear relationship between ozone uptake and the daily rate of gross photosynthesis (Equation 5; Figure 6; Ewert and Porter, 2000).).

$$GAI\_fO_{3,s(h)} = \begin{cases} 1 & if\ UO_{>FO3crit} \le \frac{\gamma_1}{\gamma_2} \\ 1-\gamma_1-\gamma_2 UO_{>FO3crit} & if\ \frac{\gamma_1}{\gamma_2} < UO_{>FO3crit} < \frac{1+\gamma_1}{\gamma_2} \\ 0 & if\ UO_{>FO3crit} \ge \frac{1+\gamma_1}{\gamma_2} \end{cases} \quad [5]$$

Where: $UO_{>FO3crit}$ (nmol m^{-2} s^{-1}) is the instantaneous O_3 leaf uptake rate (Equation 1); γ_1 (unit less; default = 0.06) and γ_2 ((nmol m^{-2} s^{-1})$^{-1}$; default = 0.0045) represent short-term damage coefficients empirically determined.

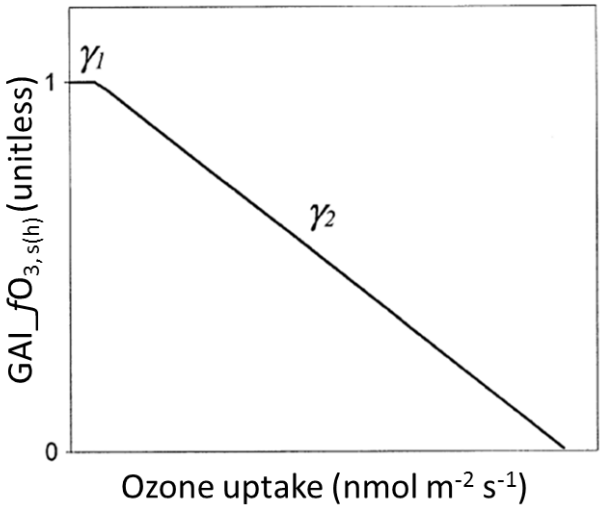

Figure 6. Relationship between factor accounting for short-term ozone effect on the daily rate of gross photosynthesis (GAI_$fO_{3,s(h)}$) and ozone uptake.

Hourly damage factors (GAI_$fO_{3,s(h)}$) computed for daylight hours are then aggregated in a daily reduction factor (GAI_$fO_{3,s(d)}$) for GAI units of the same age, considering both the damage caused by ozone during the previous hour (GAI_$fO_{3,s(h-1)}$) and recovery from ozone injury of the previous day (GAI_$rO_{3,s}$), as shown in Equation 6.

$$GAI\_fO_{3,s(d)} = \begin{cases} GAI\_fO_{3,s(h)} \cdot GAI\_fO_{3,s(h-1)} & for\ h = 1 + a..n + 1 \\ GAI\_fO_{3,s(h)} \cdot GAI\_rO_{3,s} & for\ h = 1 \end{cases} \quad [6]$$

Where: a (h) is the first sunshine hour in the day; n (h) is the total number of sunshine hours in the day.

Since the plants are recovering from ozone damages of ozone during the night, the incomplete recovery from ozone damage (GAI_$rO_{3,s}$) of the previous day is considered in the calculation of ozone effect on daily rates of CH_2O assimilation of the following day and it is dependent on leaf age (Equation 7; Figure 7).

$$GAI\_rO_{3,s} = GAI\_fO_{3,s(d-1)} + \left(1 - GAI\_fO_{3,s(d-1)}\right) GAI\_f_{LA} \quad [7]$$

Where: GAI_f_{LA} (1 = maximum recovery ability from ozone damage; 0 no recovery; unit less) is a factor accounting for leaf age and is computed over the life span of the GAI units.

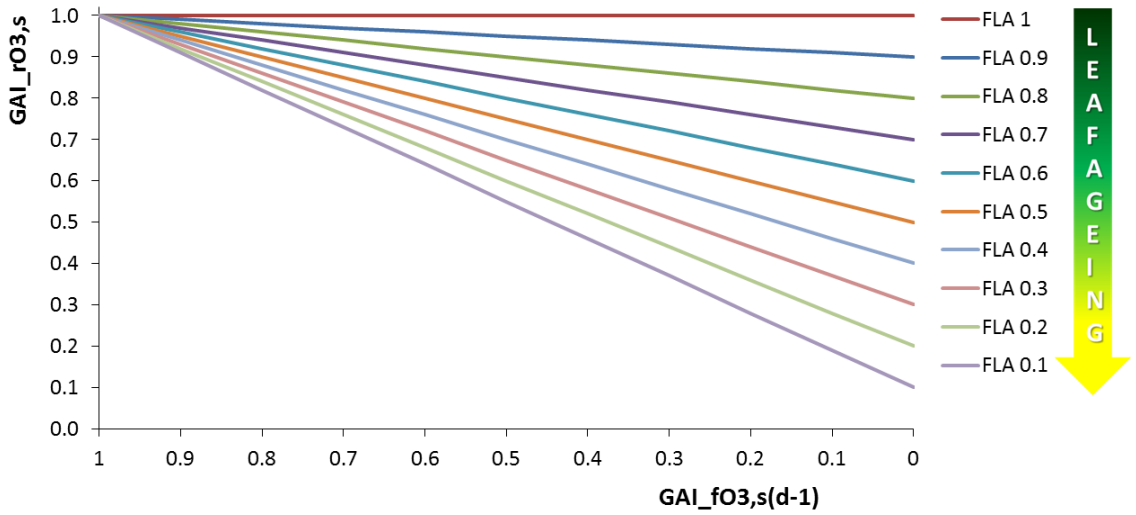

Figure 7. Recovery rates ozone injury factor ($GAI\_rO_{3,s}$,unitless) as function of the short-term daily damage factors of the previous day ($GAI\_f_{O3,s(d)}$, unitless) and leaf age (GAI_f_{LA}, unitless).

While young leaves can fully repair from O_3 damage, the recover capacity decreases linearly with the ageing of the leaves up to zero when the leaf is dead (Equation 8; Figure 8).

$$GAI\_f_{LA} = \begin{cases} 1 & if\ GAI\_PHYSDEL = 0 \\ 1 - \dfrac{GAI\_PHYSDEL}{GAI\_SPAN} & if\ 0 < GAI\_PHYSDEL < GAI\_SPAN \\ 0 & if\ GAI\_PHYSDEL \geq GAI\_SPAN \end{cases} \quad [8]$$

Where: GAI_PHYSDEL (d) represents the physiological age of a representative leaf belonging to a given GAI unit; GAI_SPAN (d) is the life span of a representative leaf belonging to a given GAI unit.

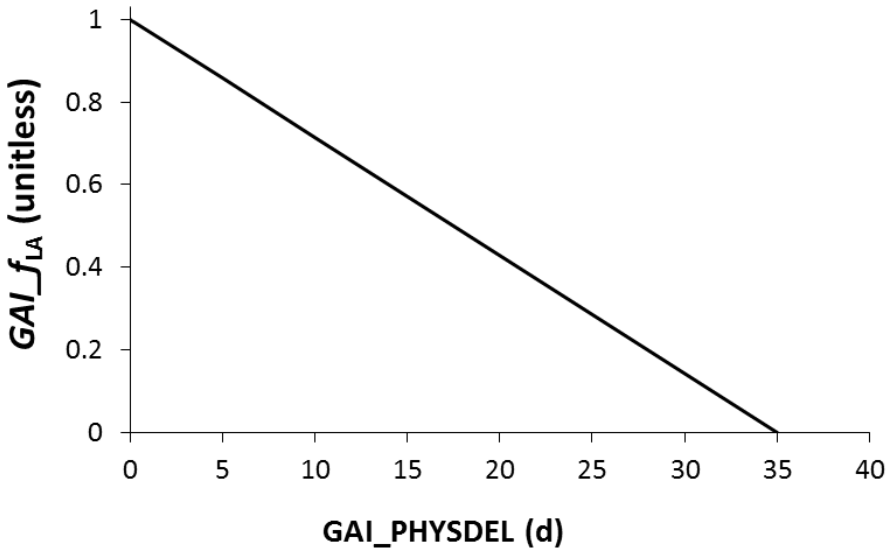

Figure 8. Relationship between factor used to simulate the recovery from ozone damage dependent on leaf age (GAI_*f*LA) and the thermal life-span of a representative leaf belonging to a given GAI unit.

An average short-term daily effect (Average_GAI_$fO_{3,s(d)}$) is computed by averaging all daily reduction factors (GAI_$fO_{3,s(d)}$, specific for each contemporaneous GAI unit) and is then applied to reduce the gross photosynthesis rate calculated by WOFOST.

$$DGAR = DGAR \cdot \text{Average\_GAI\_}fO_{3,s(d)} \quad [9]$$

Where: DGAR (Kg ha^{-1} d^{-1}) represents the actual daily gross CH_2O assimilation rate.

4.4.2.2. Long-term response and acceleration of leaf senesce due to O_3 exposure

Both the signal for the onset of senescence and the rate of senescence are computed daily for each contemporaneous GAI unit using reducing factors (GAI_$fO_{3,l}$, 0 = maximum reduction; 1 = no effect; unit less) calculated as function of cumulative ozone uptake (Equation 10).

$$GAI\_fO_{3,l} = 1 - \gamma_3 \int_0^{t=GAI\_SPAN} \frac{UO_{>FO3crit}}{1000} \cdot h_{daylight} \quad [10]$$

Where: γ_3 ((µmol m^{-2})$^{-1}$; default = 0.5) is an ozone long-term damage coefficient, empirically determined, describing the reduction in the lifetime of a mature leaf per unit of ozone accumulated uptake; $UO_{>FO3crit}$ (nmol m^{-2} s^{-1}) is the instantaneous O_3 leaf uptake rate (Equation 1); $h_{daylight}$ (h) are the sunshine hours in a given day.

Then the factor accounting for the effect of leaf senescence on daily rate of gross photosynthesis (Figure 9) is calculated as,

$$GAI\_f_{LS} = \begin{cases} 1 & if\ GAI\_PHYSDEL \le t_{l,ep} \\ \max\left[\left(1 - \dfrac{GAI\_PHYSDEL - t_{l,ep}}{\dfrac{GAI\_SPAN}{GAI\_fO_{3,l}} - t_{l,ep}}\right), 0\right] & if\ t_{l,ep} < GAI\_PHYSDEL < GAI\_SPAN \\ 0 & if\ GAI\_PHYSDEL \ge GAI\_SPAN \end{cases} \quad [11]$$

Where: $t_{l,ep}$ = 0.33 GAI_SPAN (d) are the days during which a representative leaf belonging to a given GAI unit is fully expanded.

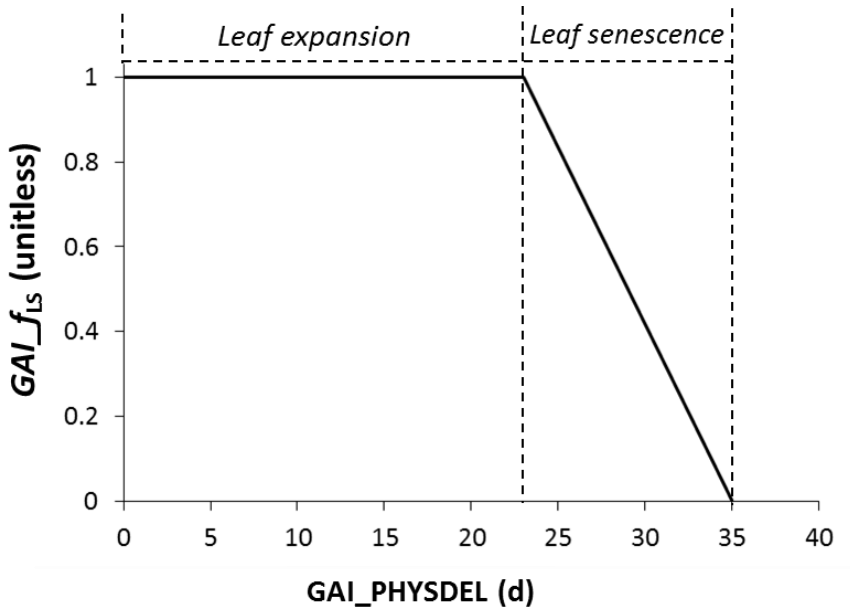

Figure 9. Relationship between factor used to simulate the decline in the daily rate of gross photosynthesis in senescing leaves (GAI_*f*LS) and the thermal life-span of a representative leaf belonging to a given GAI unit

Finally, an average long-term daily effect (Average_GAI_f_{LS}) is computed by averaging the sum of all daily reduction factor (GAI_f_{LS}) on the total number of contemporaneous age classes.

Since decreases in daily rate of gross photosynthesis are implicitly induced by the reduction in green leaf area indices (GAIs) daily associated to the faster ageing of each contemporaneous class of GAI units, the Average_GAI_f_{LS} factor is not applied to further reduce the actual daily gross CH_2O assimilation rate calculated by WOFOST in the modelling solution (Equation 9). The rationale for this is to reduce the risk of markedly overestimating the effect of senescence on reducing photosynthesis rates, double counting its impact on plant growth.

The effect of leaf senescence acceleration is computed daily in the ozone module by increasing the physiological age of all the contemporaneous GAI units (GAI_PHYSDEL) according to the Equation 12.

$$GAI\_PHYSDEL = GAI\_PHYSDEL_{(t-1)} + \max\left(GAI\_SPAN_{Adj(t-1)} - GAI\_SPAN_{Adj(t)}, 0\right) \quad [12]$$

Where: $GAI\_SPAN_{Adj(t)}$ (d) is the life span of a given GAI unit modified by the ageing effect of cumulative ozone; $GAI\_SPAN_{Adj(t-1)}$ (d) is the adjusted life span of the previous day.

Each day $GAI\_SPAN_{Adj(t)}$ is calculated via Equation 13 and then used to update the WOFOST GAIage state variables of the following day.

$$GAI\_SPAN_{Adj(t)} = GAI\_SPAN_{Adj(t-1)} \cdot GAI_{fO3,l} \quad GAI\_SPAN_{Adj(t)} = GAI\_SPAN_{Adj(t-1)} \cdot GAI_{fO3,l} \quad [13]$$

The metacodes referring to the algorithms implemented for the short- and long-term effects are reported in Appendix B and C respectively.

4.5. Daily outputs

At the end of each simulation run, daily outputs of the CropML_SoilW_AbioticDamage_solution are stored in .xls files and can be displayed via the Graphic Data Display (GDD) user interface application (http://agsys.cra-cin.it/tools/gdd/help/). Four different production levels are considered and results achieved for each of them are saved, separately in a dedicated sheet. This methodological choice allows to gain insight into the modeled effect of ozone damage on crop growth and productivity. The levels are:

1 **WL_No O_3**: it takes into account just water stress limitations to crop growth without considering any O_3 influence on crop phenology and productivity. Main daily outputs stored involve:
   - above ground biomass (AGB; Kg ha^{-1});
   - storage organs biomass (STO; Kg ha^{-1});
   - green lai index (GAI; m^{-2} m^{-2});
   - soil water content (SWC; m^{-3} m^{-3});
   - water stress index (WSI; unit less);
   - rooting depth (RD; m).

2 **WL_O_3 Long**: it takes into account water stress limitations in conjunction with the O_3 long-term effect on crop growth and leaf senescence. Short-term O_3 effect is not considered. Main daily outputs stored involve:
   - AGB_Long (Kg ha^{-1});
   - STO_Long (Kg ha^{-1});
   - GAI_Long (m^{-2} m^{-2});
   - SWC_Long (m^{-3} m^{-3});
   - WSI_Long (unit less);
   - RD_Long (m);
   - O_3 flux to stomata (O_3FluxTOStomata_Long; nmol m^{-2} s^{-1});
   - Effect of water stress on stomatal conductance (Ks_Long; unitless);
   - Percentage reduction of daily CH_2O assimilation rate (%AssReduction_Long; %).

3 **WL_O_3 Short**: it takes into account water stress limitations in conjunction with the O_3 short-term effect on crop growth and leaf senescence. Long-term O_3 effect is not considered. Main daily outputs stored involve:
   - AGB_Short (Kg ha^{-1});
   - STO_Short (Kg ha^{-1});
   - GAI_Short (m^{-2} m^{-2});
   - SWC_Short (m^{-3} m^{-3});
   - WSI_Short (unit less);
   - RD_Short (m);
   - O_3FluxTOStomata_Short (nmol m^{-2} s^{-1});
   - Ks_Short (unitless);
   - %AssReduction_Short (%).

4 **WL_O_3 Short x Long**: it takes into account water stress, long- and short-term O_3 limitations to growth and development. Main daily outputs stored involve:

- AGB_Short x Long (Kg ha^{-1});
- STO_Short x Long (Kg ha^{-1});
- GAI_Short x Long (m^{-2} m^{-2});
- SWC_Short x Long (m^{-3} m^{-3});
- WSI_Short x Long (unit less);
- RD_Short x Long (m);
- O_3FluxTOStomata_Short x Long (nmol m^{-2} s^{-1});
- Ks_Short x Long (unitless);
- %AssReduction_Short x Long (%).

As an example, some results about the simulated impact of short- and long term O_3 exposure on wheat AGB and STO are presented in Figure 10, where two contrasting regimes of ozone concentration are compared.

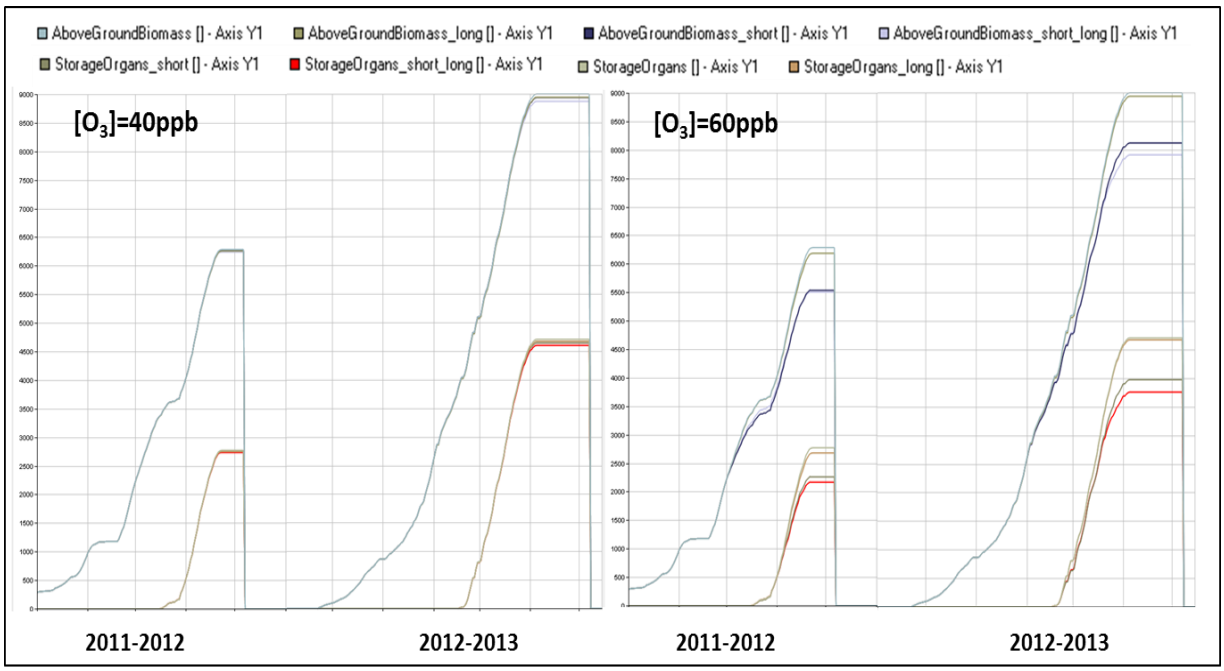

Figure 5. Graphic Data Display (GDD) interface showing aboveground biomass (kg ha^{-1}) and storage organs biomass (kg ha^{-1}) of wheat (water limited, Long-term O_3 limited, short term O_3 limited and with all limitations) simulated under two contrasting regimes of ozone concentration in a sample site of Northern Italy (seasons 2011-2012 and 2012-2013) with the CropML_SoilW_AbioticDamage_solution.

While crop productivity is slightly affected under the low-impact O_3 concentration regardless the production level considered, a decline in both AGB and STO up to -20:-25% is simulated under the enriched O_3 scenario, with differences depending on the variable and production level analyzed.

The percentage reduction of daily CH_2O assimilation triggering the STO and AGB losses under the highest O_3 concentration are shown in Figure 11, where %AssReduction_Short x Long data are plotted against O_3FluxTOStomata_Short x long (nmol m^{-2} s^{-1}).

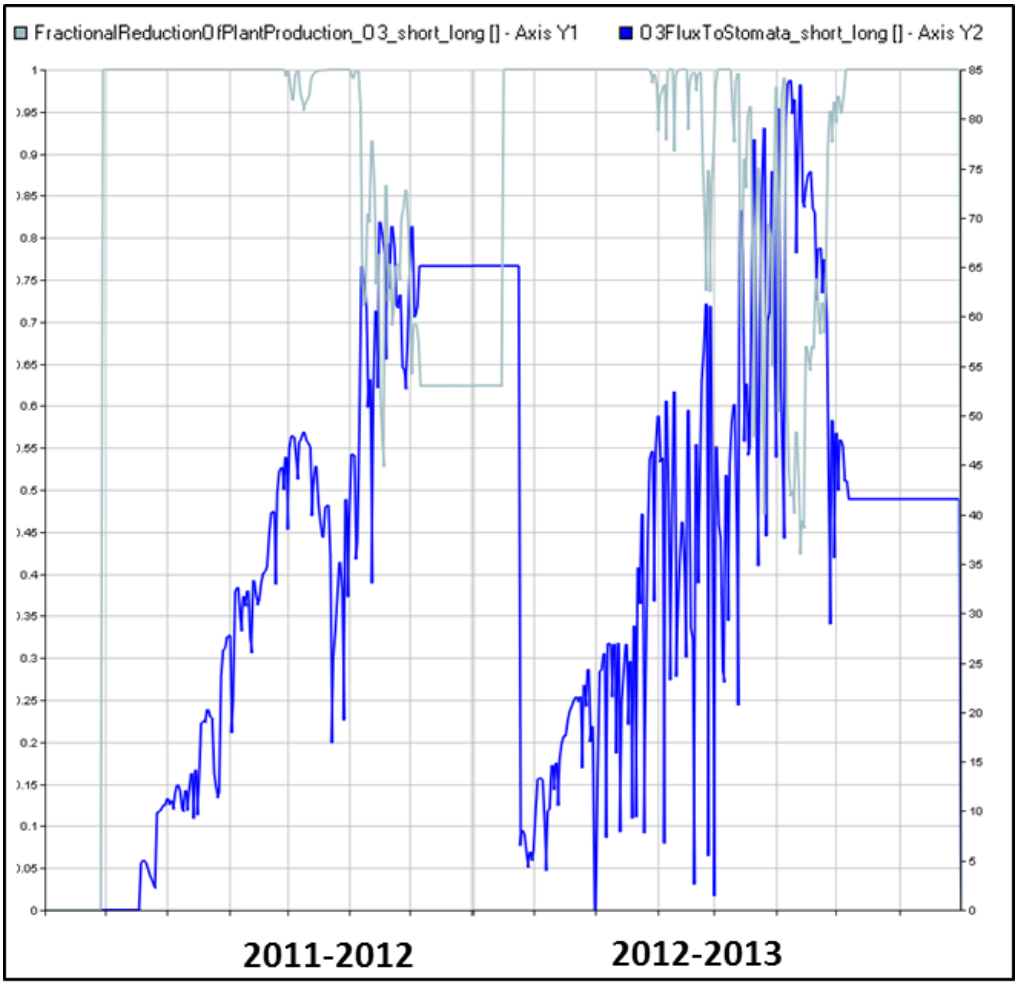

Figure 6. Graphic Data Display (GDD) interface showing the percentage reduction of daily CH_2O assimilation rate (%, light blue) against O_3 fluxes to stomata (nmol m^{-2} s^{-1}; bue) simulated under enriched O_3 concentration (60 ppb) for the limited production level (seasons 2011-2012 and 2012-2013).

As it can be noticed, O_3 fluxes to stomata frequently exceeded a threshold for damage in the growing season 2012-2013 causing decreases in daily assimilation rate up to 60 %, whereas in 2011-2012 reductions in assimilation rates were mainly confined toward the end of the season. Daily fluctuations in O_3 fluxes to stomata strictly depend on aerodynamic boundary layer resistance and stomatal conductivity, as influenced by intercepted solar radiation, O_3 effect and water stress.

A picture of the effect of water stress on stomatal conductivity and its relationships with O_3 fluxes to stomata are shown in Figure 12.

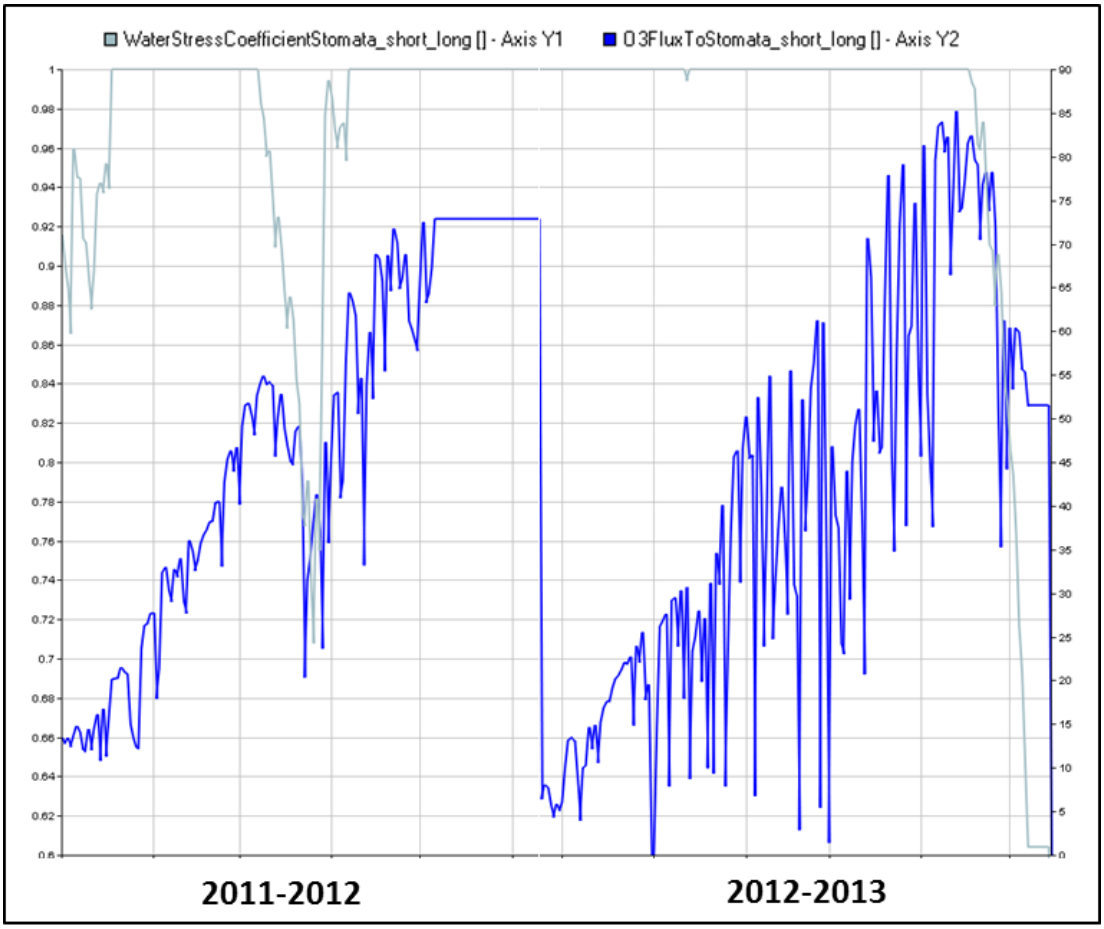

Figure 7. Graphic Data Display (GDD) interface showing the effect of water stress on stomatal conductance (Ks_Long; unitless; light blue) O_3 fluxes to stomata (nmol m^{-2} s^{-1}; bue) simulated under enriched O_3 concentration (60 ppb) for the all limited production level (seasons 2011-2012 and 2012-2013).

The water stress-induced reduction of stomatal conductance simulated in the first part of the season largely contributed to protect the crop from O_3 damage in 2011-2012, whereas in the following season the crop had less benefit from this mechanism, due to the higher amount of rainfall and soil water content in the rooted zone (Figure 13).

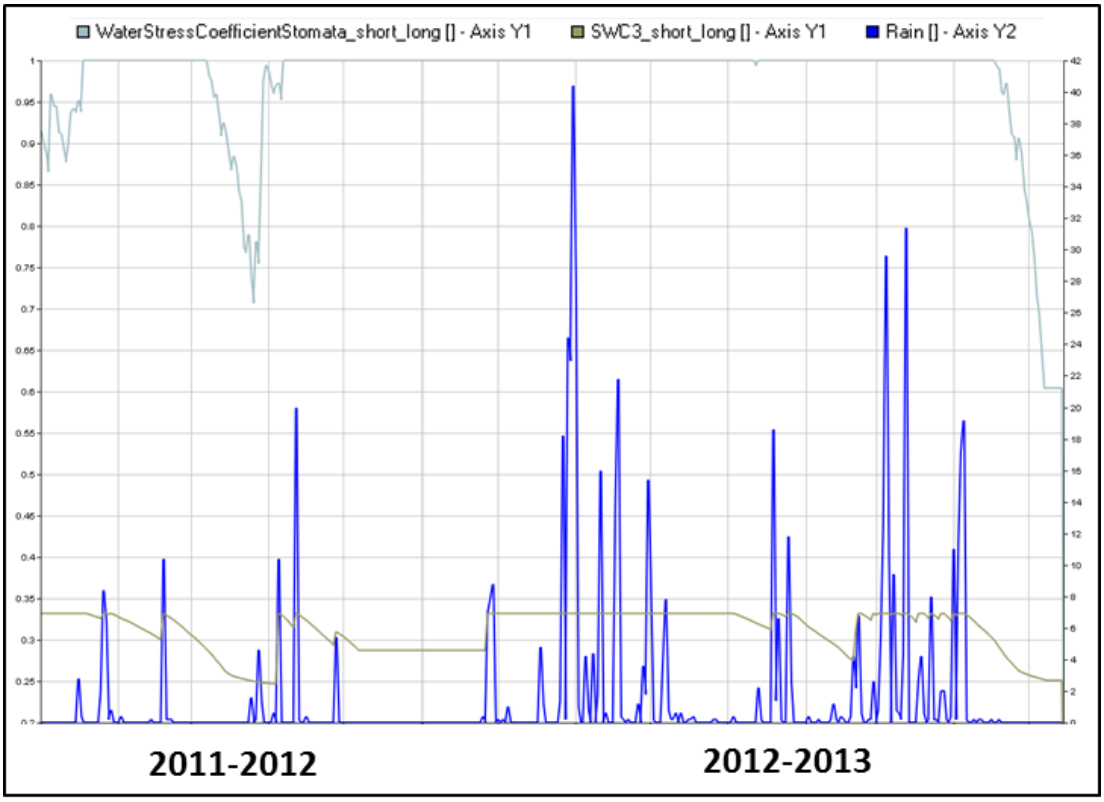

Figure 8. Graphic Data Display (GDD) interface showing the effect of water stress on stomatal conductance (Ks_Long; unitless; light blue), daily rainfall patterns (mm) and the soil water content in the rooted zone (mm) simulated under enriched O_3 concentration (60 ppb) for the all limited production level (seasons 2011-2012 and 2012-2013).

To conclude, a synthetic overview of possible fluctuations of O_3 fluxes to stomata and of percentage reduction of daily CH_2O assimilation rate as function of the variation of ozone short-term damage coefficients γ_1 and γ_2.(Equation 5) are shown in Figure 14; the flux of 90 nmol m^{-2} s^{-1} was selected since coherent with those simulated in figure 13 and 14.

Flux to stomata *(nmol m^{-2} s^{-1})*

γ_2/γ_1	0.05	0.1	0.15	0.2	0.25	0.3	0.35	0.4	0.45	0.5	0.55	0.6	0.65	0.7	0.75	0.8	0.85	0.9	0.95	1
0.0005	100	200	300	400	500	600	700	800	900	1000	1100	1200	1300	1400	1500	1600	1700	1800	1900	2000
0.001	50	100	150	200	250	300	350	400	450	500	550	600	650	700	750	800	850	900	950	1000
0.0015	33.33333	66.66667	100	133.3333	166.6667	200	233.3333	266.6667	300	333.3333	366.6667	400	433.3333	466.6667	500	533.3333	566.6667	600	633.3333	666.6667
0.002	25	50	75	100	125	150	175	200	225	250	275	300	325	350	375	400	425	450	475	500
0.0025	20	40	60	80	100	120	140	160	180	200	220	240	260	280	300	320	340	360	380	400
0.003	16.66667	33.33333	50	66.66667	83.33333	100	116.6667	133.3333	150	166.6667	183.3333	200	216.6667	233.3333	250	266.6667	283.3333	300	316.6667	333.3333
0.0035	14.28571	28.57143	42.85714	57.14286	71.42857	85.71429	100	114.2857	128.5714	142.8571	157.1429	171.4286	185.7143	200	214.2857	228.5714	242.8571	257.1429	271.4286	285.7143
0.004	12.5	25	37.5	50	62.5	75	87.5	100	112.5	125	137.5	150	162.5	175	187.5	200	212.5	225	237.5	250
0.0045	11.11111	22.22222	33.33333	44.44444	55.55556	66.66667	77.77778	88.88889	100	111.1111	122.2222	133.3333	144.4444	155.5556	166.6667	177.7778	188.8889	200	211.1111	222.2222
0.005	10	20	30	40	50	60	70	80	90	100	110	120	130	140	150	160	170	180	190	200
0.0055	9.090909	18.18182	27.27273	36.36364	45.45455	54.54545	63.63636	72.72727	81.81818	90.90909	100	109.0909	118.1818	127.2727	136.3636	145.4545	154.5455	163.6364	172.7273	181.8182
0.006	8.333333	16.66667	25	33.33333	41.66667	50	58.33333	66.66667	75	83.33333	91.66667	100	108.3333	116.6667	125	133.3333	141.6667	150	158.3333	166.6667
0.0065	7.692308	15.38462	23.07692	30.76923	38.46154	46.15385	53.84615	61.53846	69.23077	76.92308	84.61538	92.30769	100	107.6923	115.3846	123.0769	130.7692	138.4615	146.1538	153.8462
0.007	7.142857	14.28571	21.42857	28.57143	35.71429	42.85714	50	57.14286	64.28571	71.42857	78.57143	85.71429	92.85714	100	107.1429	114.2857	121.4286	128.5714	135.7143	142.8571
0.0075	6.666667	13.33333	20	26.66667	33.33333	40	46.66667	53.33333	60	66.66667	73.33333	80	86.66667	93.33333	100	106.6667	113.3333	120	126.6667	133.3333
0.008	6.25	12.5	18.75	25	31.25	37.5	43.75	50	56.25	62.5	68.75	75	81.25	87.5	93.75	100	106.25	112.5	118.75	125
0.0085	5.882353	11.76471	17.64706	23.52941	29.41176	35.29412	41.17647	47.05882	52.94118	58.82353	64.70588	70.58824	76.47059	82.35294	88.23529	94.11765	100	105.8824	111.7647	117.6471
0.009	5.555556	11.11111	16.66667	22.22222	27.77778	33.33333	38.88889	44.44444	50	55.55556	61.11111	66.66667	72.22222	77.77778	83.33333	88.88889	94.44444	100	105.5556	111.1111
0.0095	5.263158	10.52632	15.78947	21.05263	26.31579	31.57895	36.84211	42.10526	47.36842	52.63158	57.89474	63.15789	68.42105	73.68421	78.94737	84.21053	89.47368	94.73684	100	105.2632
0.01	5	10	15	20	25	30	35	40	45	50	55	60	65	70	75	80	85	90	95	100

Daily assimilation rate reduction *(1=no impact; 0=max impact; unitless) at a flux of 90 nmol m^{-2} s^{-1}*

γ_2/γ_1	0.05	0.1	0.15	0.2	0.25	0.3	0.35	0.4	0.45	0.5	0.55	0.6	0.65	0.7	0.75	0.8	0.85	0.9	0.95	1
0.0005	1	1	1	1	1	1	1	1	1	1	1	1	1	1	1	1	1	1	1	1
0.001	0.96	1	1	1	1	1	1	1	1	1	1	1	1	1	1	1	1	1	1	1
0.0015	0.915	0.965	1	1	1	1	1	1	1	1	1	1	1	1	1	1	1	1	1	1
0.002	0.87	0.92	0.97	1	1	1	1	1	1	1	1	1	1	1	1	1	1	1	1	1
0.0025	0.825	0.875	0.925	0.975	1	1	1	1	1	1	1	1	1	1	1	1	1	1	1	1
0.003	0.78	0.83	0.88	0.93	0.98	1	1	1	1	1	1	1	1	1	1	1	1	1	1	1
0.0035	0.735	0.785	0.835	0.885	0.935	0.985	1	1	1	1	1	1	1	1	1	1	1	1	1	1
0.004	0.69	0.74	0.79	0.84	0.89	0.94	0.99	1	1	1	1	1	1	1	1	1	1	1	1	1
0.0045	0.645	0.695	0.745	0.795	0.845	0.895	0.945	0.995	1	1	1	1	1	1	1	1	1	1	1	1
0.005	0.6	0.65	0.7	0.75	0.8	0.85	0.9	0.95	1	1	1	1	1	1	1	1	1	1	1	1
0.0055	0.555	0.605	0.655	0.705	0.755	0.805	0.855	0.905	0.955	1	1	1	1	1	1	1	1	1	1	1
0.006	0.51	0.56	0.61	0.66	0.71	0.76	0.81	0.86	0.91	0.96	1	1	1	1	1	1	1	1	1	1
0.0065	0.465	0.515	0.565	0.615	0.665	0.715	0.765	0.815	0.865	0.915	0.965	1	1	1	1	1	1	1	1	1
0.007	0.42	0.47	0.52	0.57	0.62	0.67	0.72	0.77	0.82	0.87	0.92	0.97	1	1	1	1	1	1	1	1
0.0075	0.375	0.425	0.475	0.525	0.575	0.625	0.675	0.725	0.775	0.825	0.875	0.925	0.975	1	1	1	1	1	1	1
0.008	0.33	0.38	0.43	0.48	0.53	0.58	0.63	0.68	0.73	0.78	0.83	0.88	0.93	0.98	1	1	1	1	1	1
0.0085	0.285	0.335	0.385	0.435	0.485	0.535	0.585	0.635	0.685	0.735	0.785	0.835	0.885	0.935	0.985	1	1	1	1	1
0.009	0.24	0.29	0.34	0.39	0.44	0.49	0.54	0.59	0.64	0.69	0.74	0.79	0.84	0.89	0.94	0.99	1	1	1	1
0.0095	0.195	0.245	0.295	0.345	0.395	0.445	0.495	0.545	0.595	0.645	0.695	0.745	0.795	0.845	0.895	0.945	0.995	1	1	1
0.01	0.15	0.2	0.25	0.3	0.35	0.4	0.45	0.5	0.55	0.6	0.65	0.7	0.75	0.8	0.85	0.9	0.95	1	1	1

Figure 9. Changes in the values of O_3 flux to stomata (nmol m^{-2} s^{-1}) and in the factor triggering the reduction of daily CH_2O assimilation rate (%) as function of different combinations of short-term damage coefficients γ_1 and γ_2

5. Preliminary results from the test conditions experiment

The preliminary results of the simulations to evaluate the sensitivity of the modelling solution to ozone exposure under the test conditions described in section 3 are reported below as:

- boxplots, to show the variability in the 20-years series of simulated outputs;
- daily dynamics, to highlight the differences in model behavior in contrasting growing seasons (e.g. high versus low impact years).

We note here, that the evaluation of the model results against observations, would need the evaluation of detailed chamber and field studies in a coherent way, which will be performed in different study.

While the seasonal outputs aim to highlight the differences among the short-, long- and short&long production levels (as explained in section 4.5) and the consecutive impacts of 0_3 damage on yield , the long-term simulations refer exclusively to the Short & Long production level and concern:

- final AGB (kg ha^{-1}), final yield (kg ha^{-1}) and maximum green leaf area index (m^2 m^{-2}) among the growth variables,
- number of days with O_3 flux exceeding the critical crop-specific O_3 concentration (d), average fractional reduction of daily gross CH_2O assimilation rate during the crop cycle (%), the cumulative O_3 fluxes during the growing season (nmol m^{-2}) among the variables triggering the O_3 damages.

5.1. Long-term simulations under different tropospheric O_3 concentrations

Figures 15-18, show yields for wheat and barley in Bremen and Jerez for different ozone conditions: 20 ppb (pre-industrial), 40 ppb (current background), and 60 ppb (polluted), the latter average over the growing season, or in specific months on top of the 40 ppb background conditions. Irrespective of ozone, rainfed wheat and barley yields are lower by only 12 % in Bremen compared to fully irrigated crops, while strongly reduced by 55 % in Jerez. Additionally, wheat yield losses, up to 30 % are calculated for ozone concentrations of 60 ppb, and only half of these for barley. Yield losses are substantially smaller in Jerez for rain-fed crops, when stomatal closure is limiting gas exchange, and thus impeding photosynthesis, crop growth and yields, but also reducing ozone uptake.

5.1.1. Final Yield

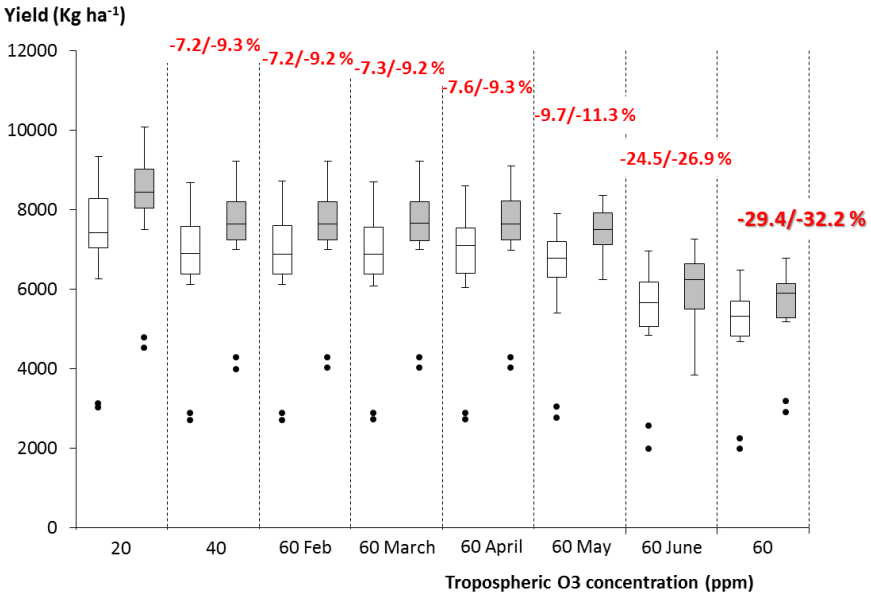

Figure 10. Boxplot of final yield values (kg ha^{-1}) simulated for the pre-industrial, background and high ozone concentrations scenarios. Each box is derived from the 19 annual values simulated for wheat crop in Bremen, Germany. Open boxes refer to rainfed; grey boxes to fully irrigated conditions. Dots represent results for the two lowest extreme years. Red numbers represent the relative reduction due to ozone compared to the 20 ppb case.

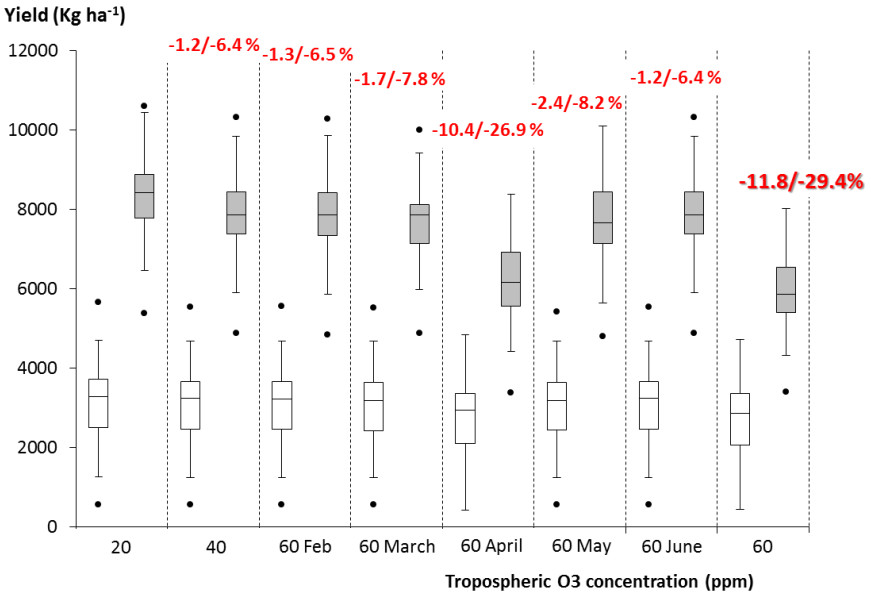

Figure 11. Boxplot of final yield values (kg ha^{-1}) simulated for the pre-industrial, back ground and high ozone concentrations scenarios. Each box is derived from the 19 values simulated for wheat crop in Jerez de la Frontera, Spain. Open boxes refer to rainfed conditions, grey boxes to fully irrigated conditions. Dots represent results for the two lowest extreme years. Red numbers represent the relative reduction due to ozone compared to the 20 ppb case.

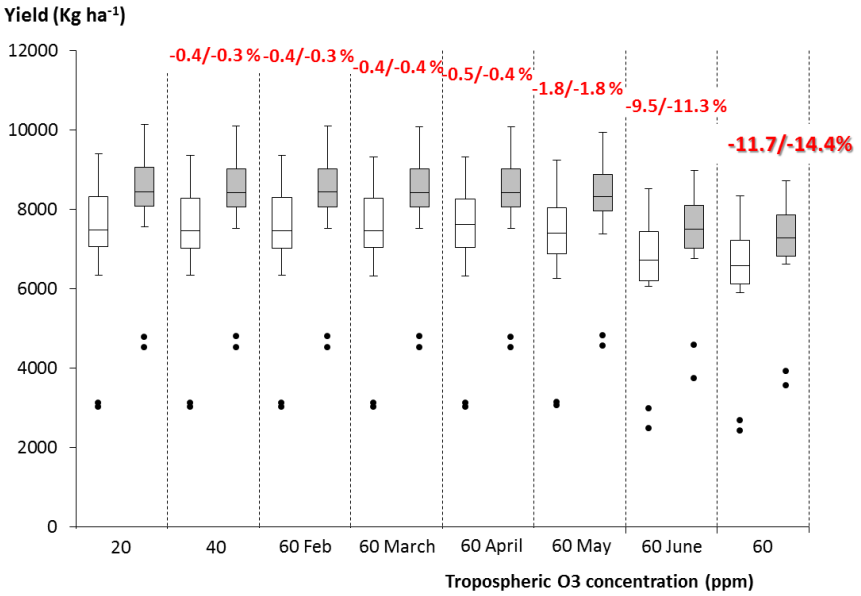

Figure 17. Boxplot of final yield values (Kg ha^{-1}) simulated for the pre-industrial, back ground and high Ozone concentrations scenarios. Each box is derived from the 19 values simulated for barley crop in Bremen, Germany. Open boxes refer to rainfed conditions, grey boxes to fully irrigated conditions. Dots represent results for the two lowest extreme years. Red numbers represent the relative reduction due to ozone compared to the 20 ppb case.

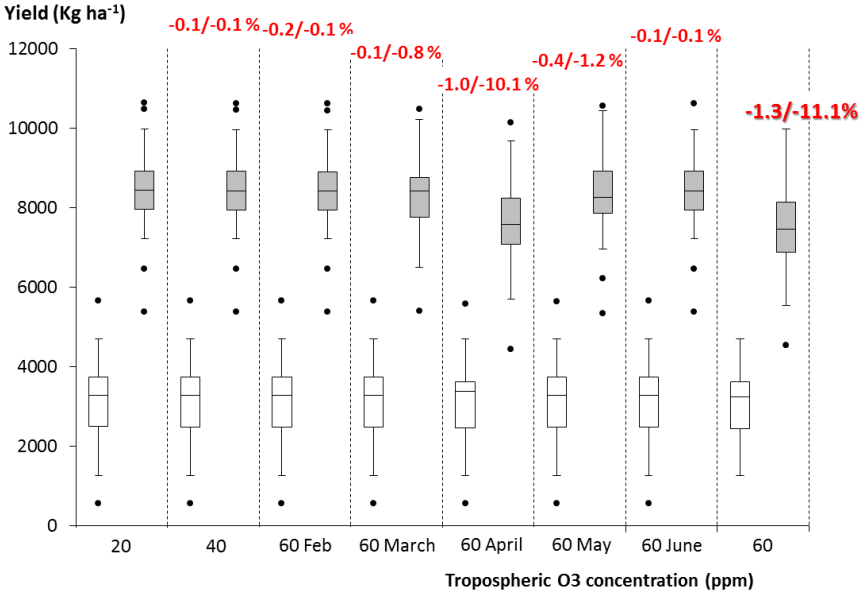

Figure 18. Boxplot of final yield values (kg ha^{-1}) simulated for the pre-industrial (20 ppb), back ground (40 ppb) and high (60 ppb) Ozone concentrations scenarios. Each box is derived from the 19 values simulated for barley crop in Jerez de la Frontera, Spain Open boxes refer to rainfed conditions, grey boxes to fully irrigated conditions. Dots represent results for the two lowest extreme years. Red numbers represent the relative reduction due to ozone compared to the 20 ppb case.

Figure 19 shows that despite different ozone impacts on crop, the 'fully irrigated' water use was not strongly affected.

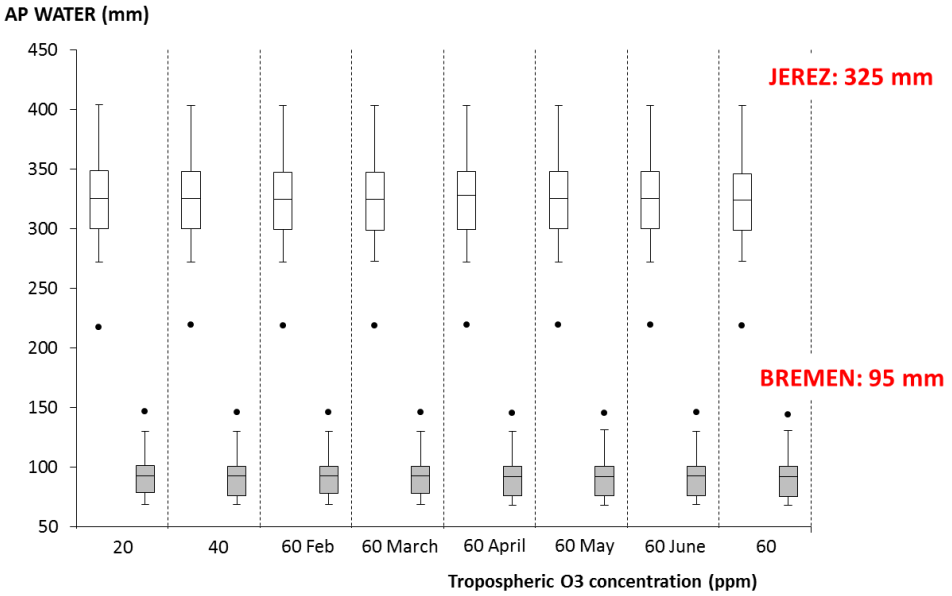

Figure 19. Boxplot of absolute amounts of water (mm) applied to wheat/barley crops during the growing seasons under the fully irrigated conditions for the pre-industrial, back ground and high Ozone concentrations scenarios. Each box is derived from the 19 values simulated for barley crop in Jerez de la Frontera, Spain. Open boxes refer Bremen, grey boxes to Jerez de la Frontera.

5.1.2. Final above ground biomass (AGB)

Figure 20-23 demonstrate that in relative terms the amount of biomass at harvest was similar to yield decline, in relative terms. Absolute biomass loss was much higher in Jerez compared to Bremen, but the relative losses were smaller in Jerez due to stomatal closure under hot conditions. Biomass losses in Barley were less than in wheat.

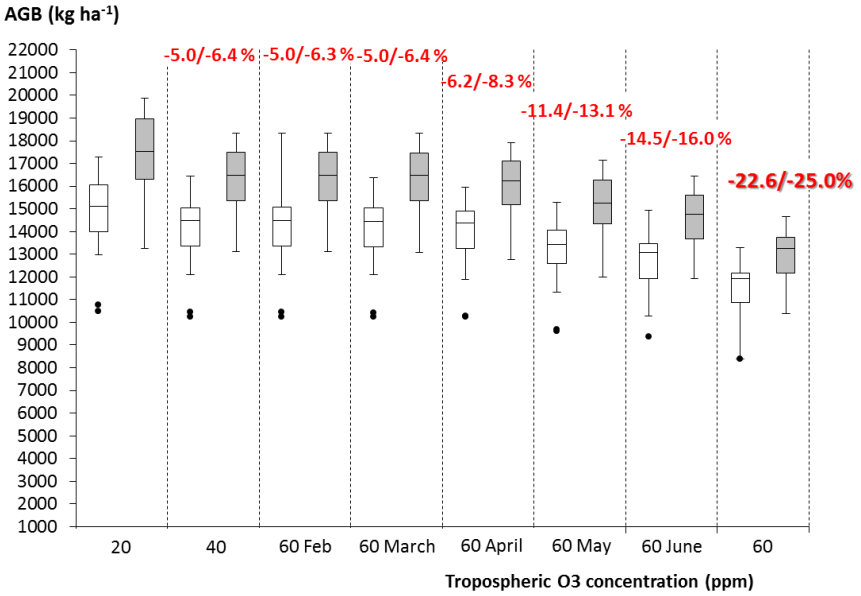

Figure 12. Boxplot of final AGB (Kg ha^{-1}) simulated for the pre-industrial, back ground and high Ozone concentrations scenarios. Each box is derived from the 19 values simulated for wheat crop in Bremen, Germany. Open boxes refer to rainfed conditions, grey boxes to fully irrigated conditions.

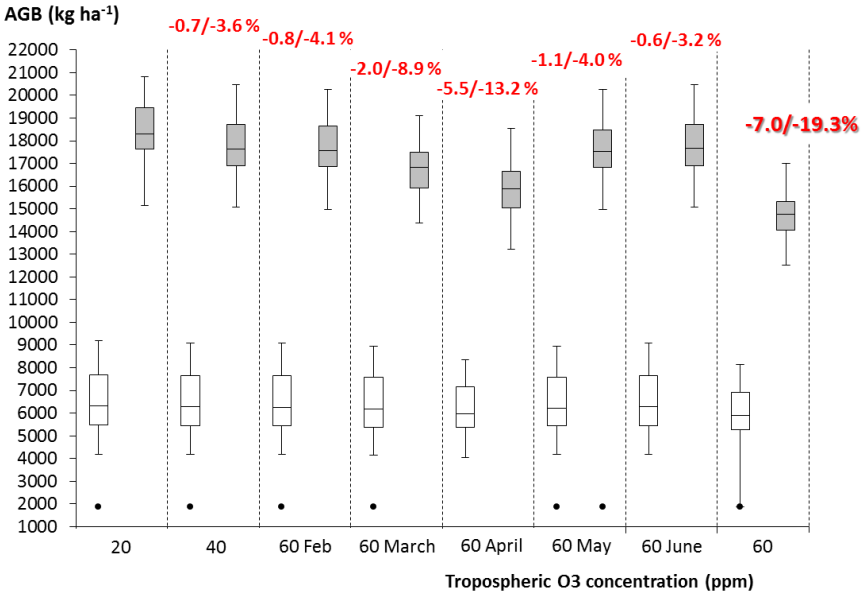

Figure 13. Boxplot of final AGB (kg ha^{-1}) simulated for the pre-industrial, back ground and high Ozone concentrations scenarios. Each box is derived from the 19 values simulated for wheat crop in Jerez de la Frontera, Spain. Open boxes refer to rainfed conditions, grey boxes to fully irrigated conditions.

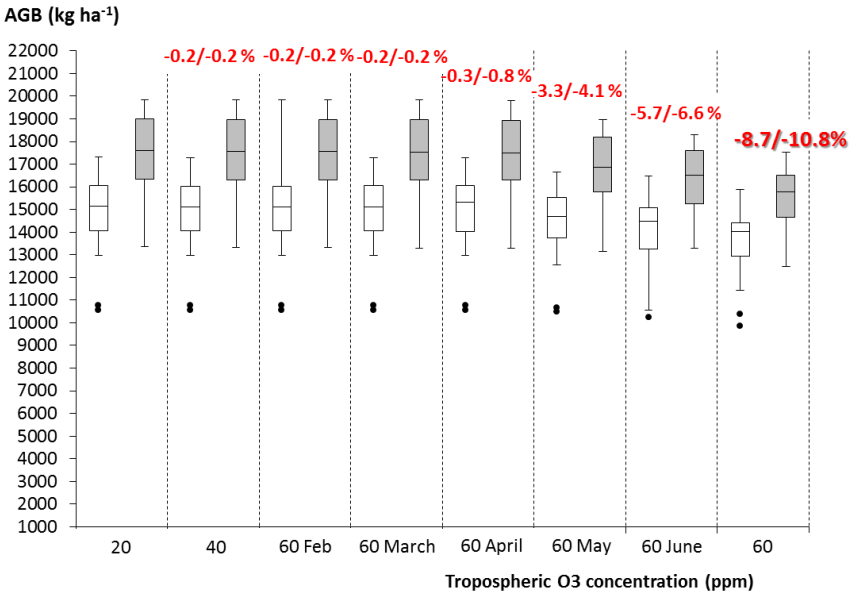

Figure 14. Boxplot of final AGB (kg ha^{-1}) simulated for the pre-industrial, back ground and high Ozone concentrations scenarios. Each box is derived from the 19 values simulated for barley crop in Bremen, Germany. Open boxes refer to rainfed conditions, grey boxes to fully irrigated conditions.

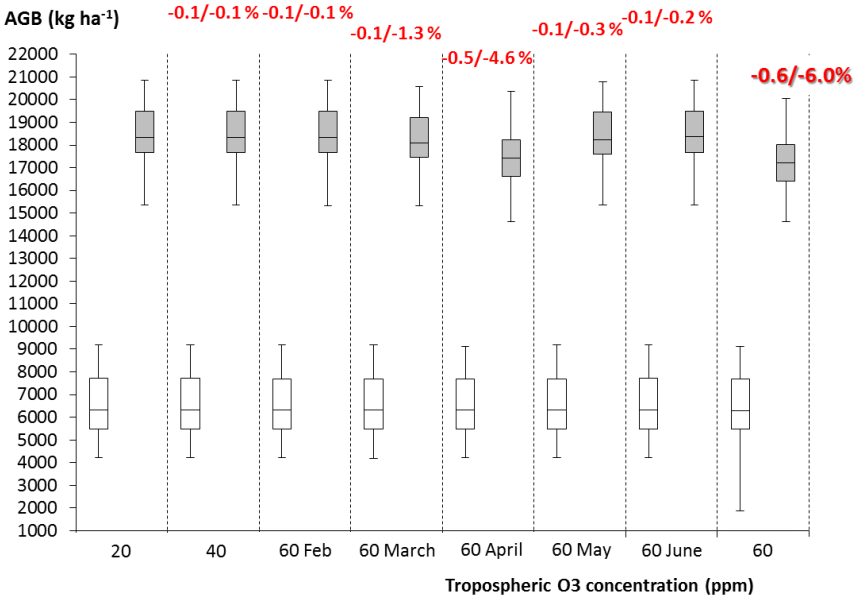

Figure 15. Boxplot of AGB (kg ha^{-1}) simulated for the pre-industrial, back ground and high Ozone concentrations scenarios. Each box is derived from the 19 values simulated for barley crop in Jerez de la Frontera, Spain. Open boxes refer to rainfed conditions, grey boxes to fully irrigated conditions.

5.1.3. Maximum green leaf area index ($GLAI_{max}$)

The green leaf area (m^2) divided by the ground area (m^2) GLAI (Figure 24-27) is an indicator for crop growth, and is usually maximizing around flowering. GLAI values are in a realistic range for all ozone cases (wheat/barley), and show substantially lower declines than biomass, indicating to a substantial amount of assimilates used for respiration/repair.

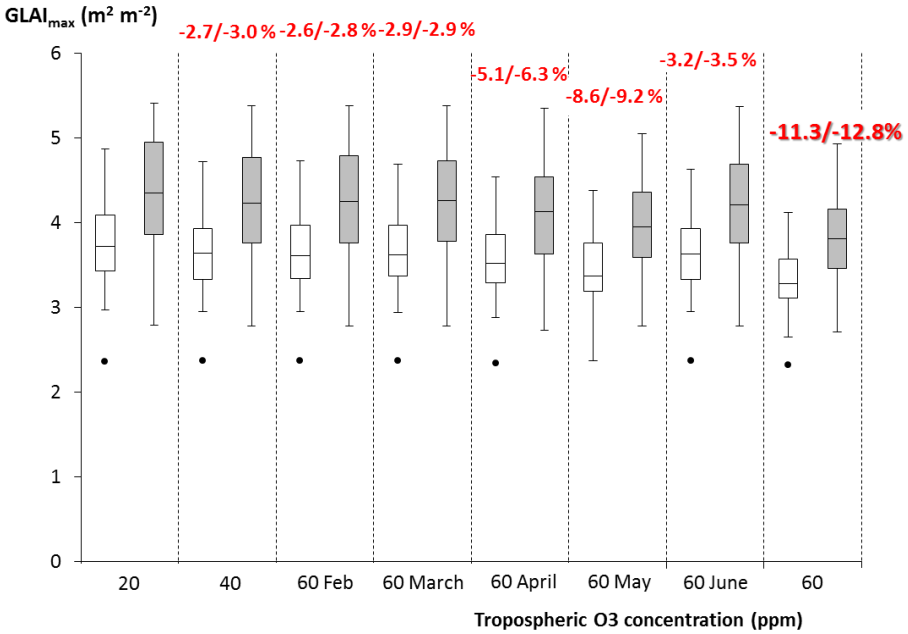

Figure 16. Boxplot of maximum GLAI (m^2 m^{-2}) simulated for the pre-industrial, back ground and high ozone concentrations scenarios. Each box is derived from the 19 values simulated for wheat crop in Bremen, Germany. Open boxes refer to rainfed conditions, grey boxes to fully irrigated conditions.

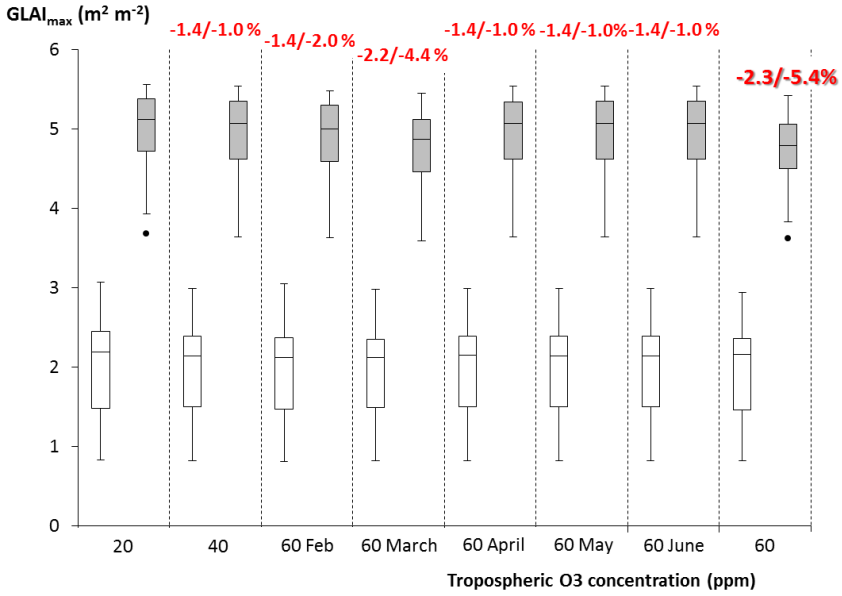

Figure 17. Boxplot of maximum GLAI (m^2 m^{-2}) simulated for the pre-industrial, back ground and high Ozone concentrations scenarios. Each box is derived from the 19 values simulated for wheat crop in Jerez de la Frontera, Spain. Open boxes refer to rainfed conditions, grey boxes to fully irrigated conditions.

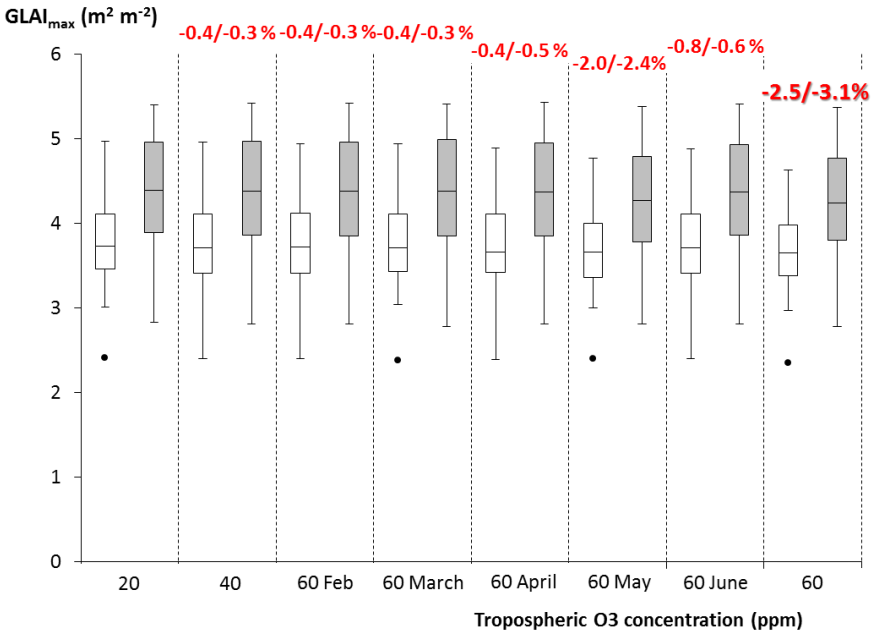

Figure 18. Boxplot of maximum GLAI (m^2 m^{-2}) simulated for the pre-industrial, back ground and high Ozone concentrations scenarios. Each box is derived from the 19 values simulated for barley crop in Bremen, Germany. Open boxes refer to rainfed conditions, grey boxes to fully irrigated conditions.

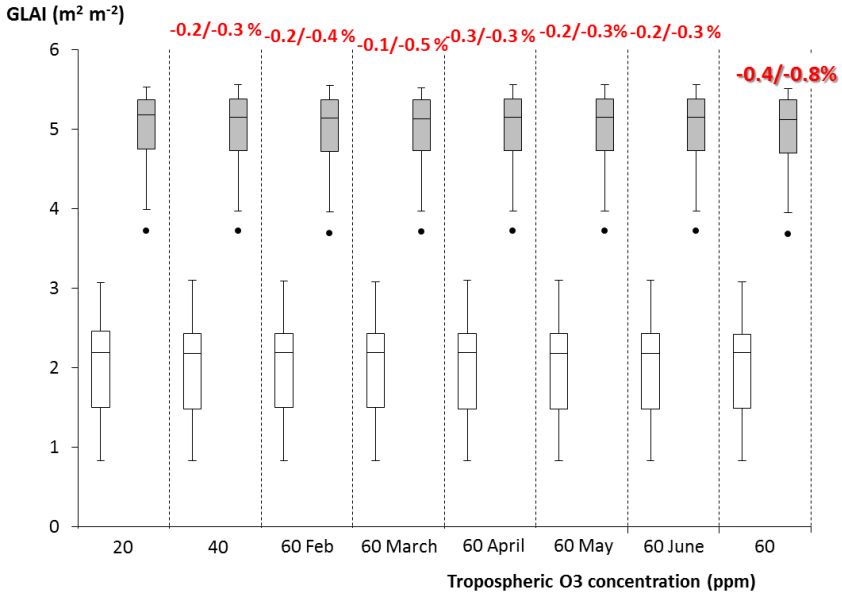

Figure 27. Boxplot of maximum GLAI (m^2 m^{-2}) simulated for the pre-industrial, back ground and high Ozone concentrations scenarios. Each box is derived from the 19 values simulated for barley crop in Jerez de la Frontera, Spain. Open boxes refer to rainfed conditions, grey boxes to fully irrigated conditions.

5.1.4. Days with O_3 flux exceeding the critical O_3 concentration (O_3 flux>O_{3crit})

Figure 28-31 show the number of days where the O3 flux is exceeding the critical thresholds, see section 4.4.2.1. Elevated (60 ppb) ozone adds approximately 5-10 additional days each month above the threshold flux, summing to 50 additional days at harvest in Bremen for wheat. At Jerez, under water limited conditions the number of days above critical ozone fluxes is quite limited, but more pronounced under irrigated conditions.

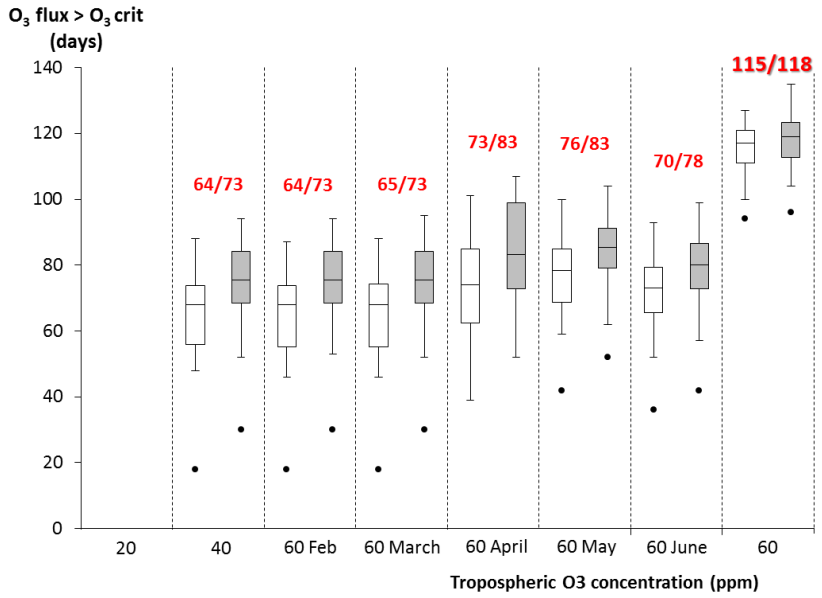

Figure 28. Boxplot of number of days with O_3 flux > O_3 crit. (days) simulated for the pre-industrial, back ground and high Ozone concentrations scenarios. Each box is derived from the 19 values simulated for wheat crop in Bremen, Germany. Open boxes refer to rainfed conditions, grey boxes to fully irrigated conditions.

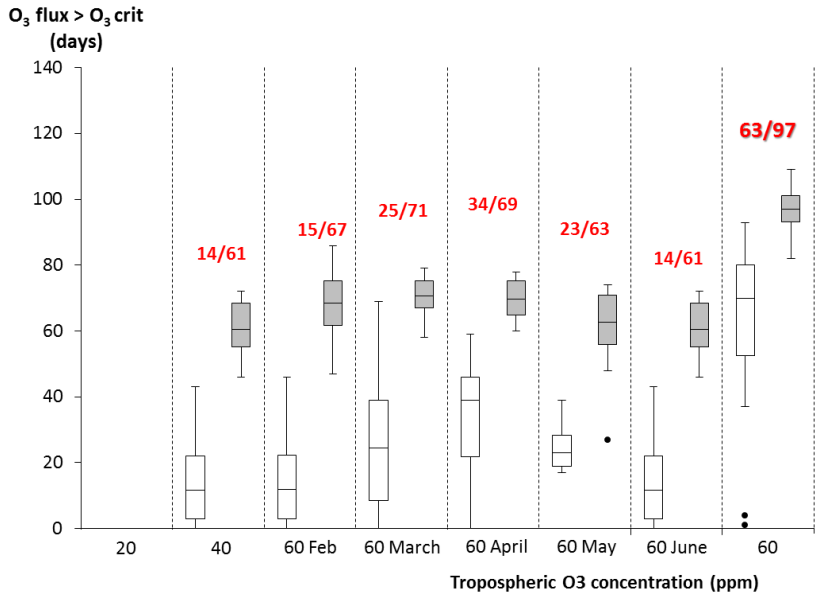

Figure 29. Boxplot of number of days with O_3 flux > O_3 crit. (days) simulated for the pre-industrial, back ground and high Ozone concentrations scenarios. Each box is derived from the 19 values simulated for wheat crop in Jerez de la Frontera, Spain. Open boxes refer to rainfed conditions, grey boxes to fully irrigated conditions.

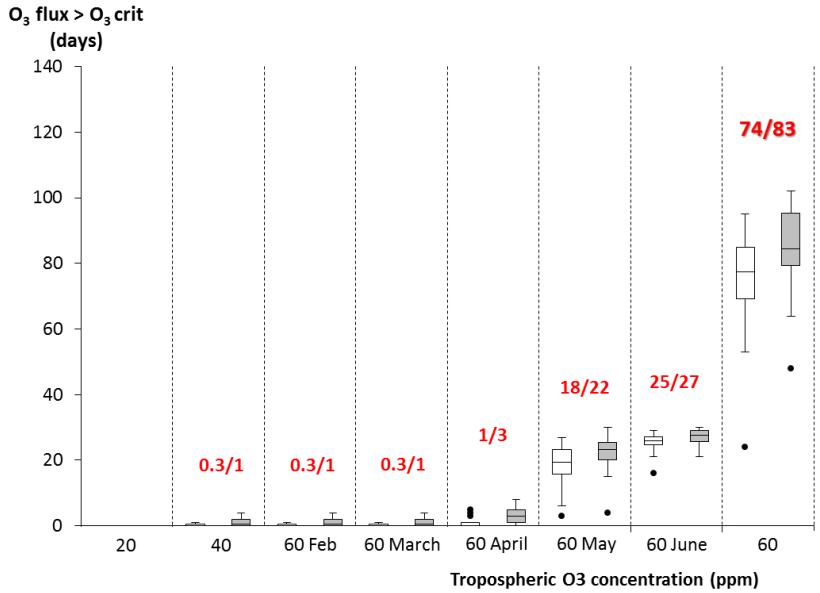

Figure 19. Boxplot of number of days with O_3 flux > O_3 crit. (days) simulated for the pre-industrial, back ground and high Ozone concentrations scenarios. Each box is derived from the 19 values simulated for barley crop in Bremen, Germany. Open boxes refer to rainfed conditions, grey boxes to fully irrigated conditions.

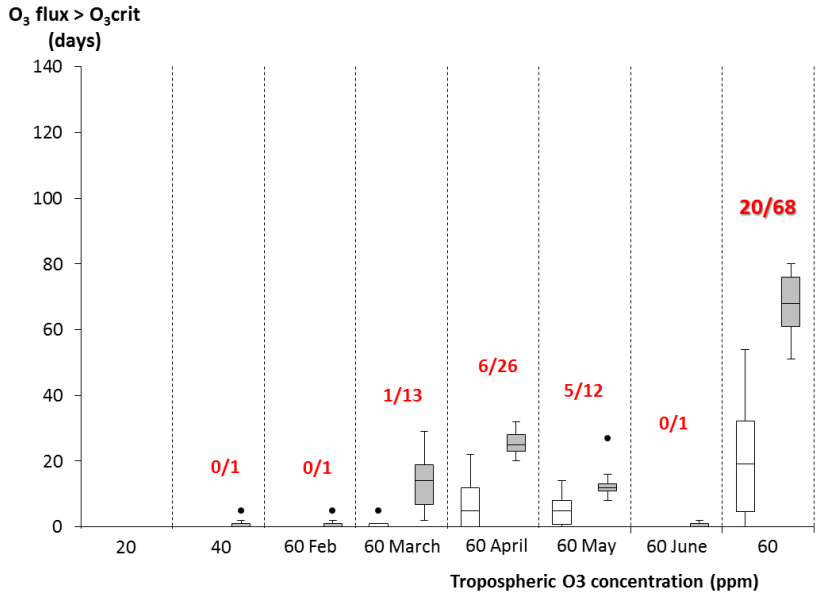

Figure 20. Boxplot of number of days with O_3 flux > O_3 crit. (days) simulated for the pre-industrial, back ground and high Ozone concentrations scenarios. Each box is derived from the 19 values simulated for barley crop in Jerez de la Frontera, Spain. Open boxes refer to rainfed conditions, grey boxes to fully irrigated conditions.

5.1.5. Mean fractional reduction of daily gross CH_2O assimilation rate (A_{max}red) within the growing season

Figure 32-35 show that CH_2O assimilation rates (A_{max}red) in wheat were reduced between 6-20 % in Bremen, and 2 and 20 % in Jerez, depending on water limited or fully irrigated conditions- in line with the reductions of biomass and green leaf area index. Likewise, in barley the reductions were much smaller.

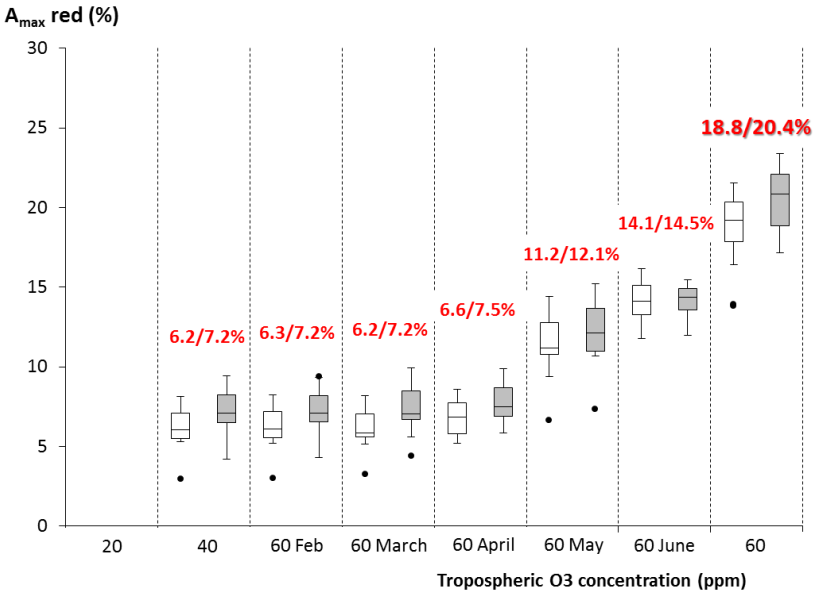

Figure 21. Boxplot of absolute mean values of A_{max}red within the growing season, simulated for the pre-industrial, back ground and high ozone concentrations scenarios. Each box is derived from the 19 values simulated for wheat crop in Bremen, Germany. Open boxes refer to rainfed conditions, grey boxes to fully irrigated conditions.

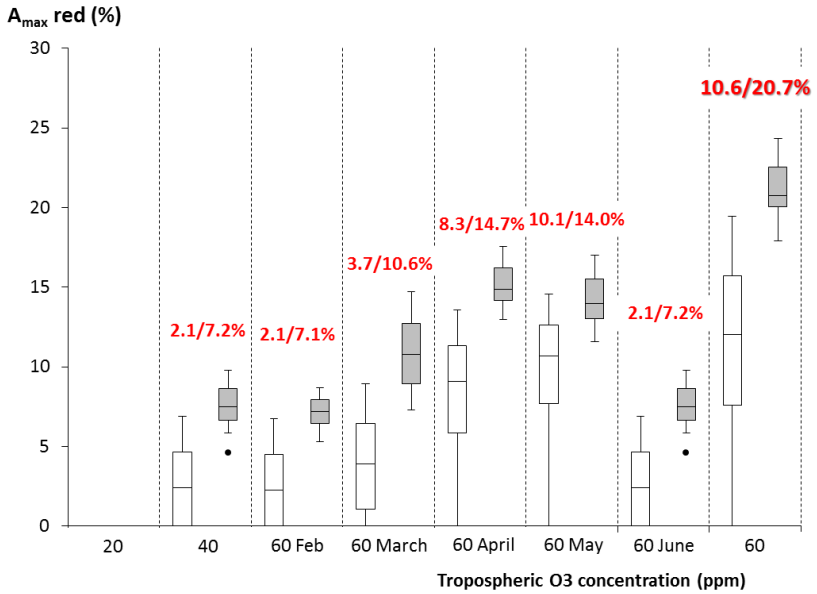

Figure 22. Boxplot of absolute mean values of A_{max}red within the growing season, simulated for the pre-industrial, back ground and high ozone concentrations scenarios. Each box is derived from the 19 values simulated for wheat crop in Jerez de la Frontera, Spain. Open boxes refer to rainfed conditions, grey boxes to fully irrigated conditions.

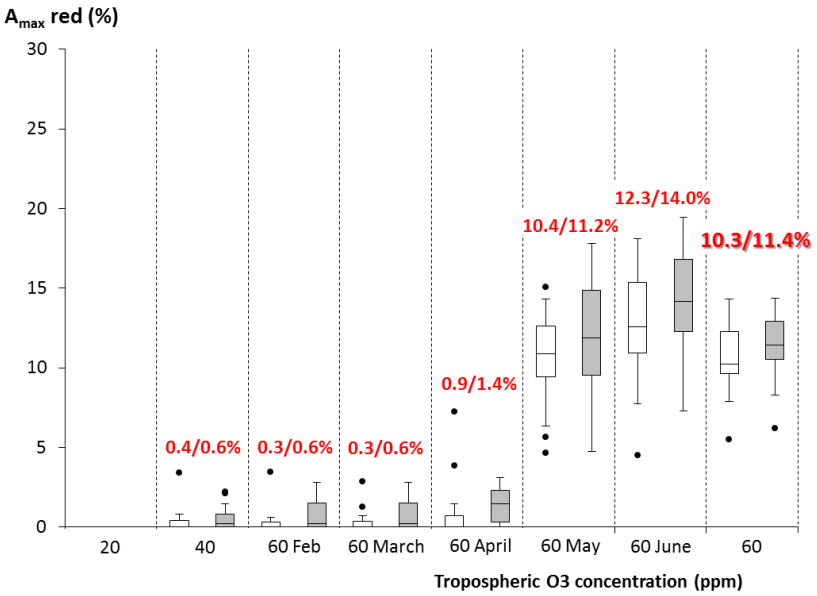

Figure 23. Boxplot of absolute mean values of A_{max}red within the growing season, simulated for the pre-industrial, back ground and high Ozone concentrations scenarios. Each box is derived from the 19 values simulated for barley crop in Bremen, Germany. Open boxes refer to rainfed conditions, grey boxes to fully irrigated conditions.

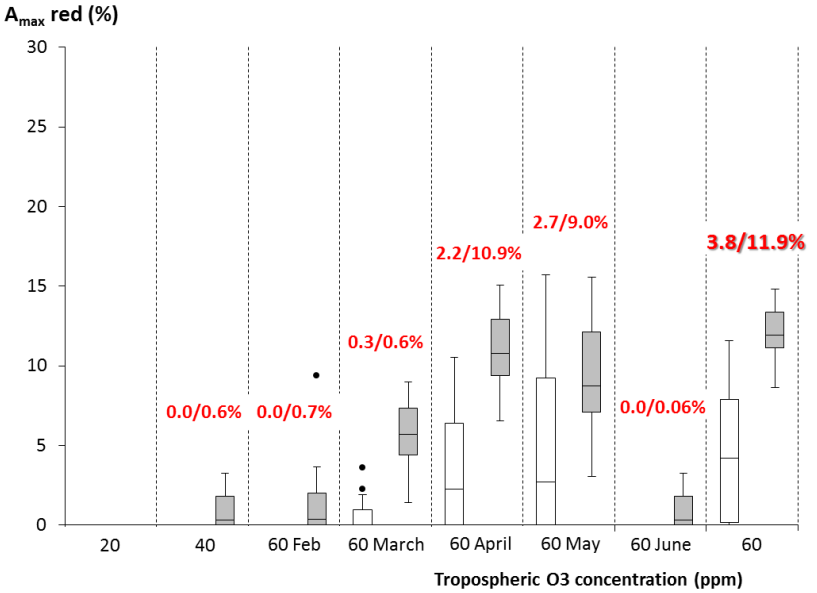

Figure 24. Boxplot of absolute mean values of A_{max}red (%) within the growing season, simulated for the pre-industrial, back ground and high Ozone concentrations scenarios. Each box is derived from the 19 values simulated for barley crop in Jerez de la Frontera, Spain. Open boxes refer to rainfed conditions, grey boxes to fully irrigated conditions.

5.1.6. Cumulative ozone fluxes during the growing season (O_3 cum fluxes)

Figure 36-39 show cumulative ozone fluxes during the growing season. As expected cumulative fluxes scale with the ozone concentrations, but are strongly down regulated under water limited conditions in Jerez. The anticipation of the growing cycle in Jerez compared to Bremen is clearly visible in the month of highest ozone flux.

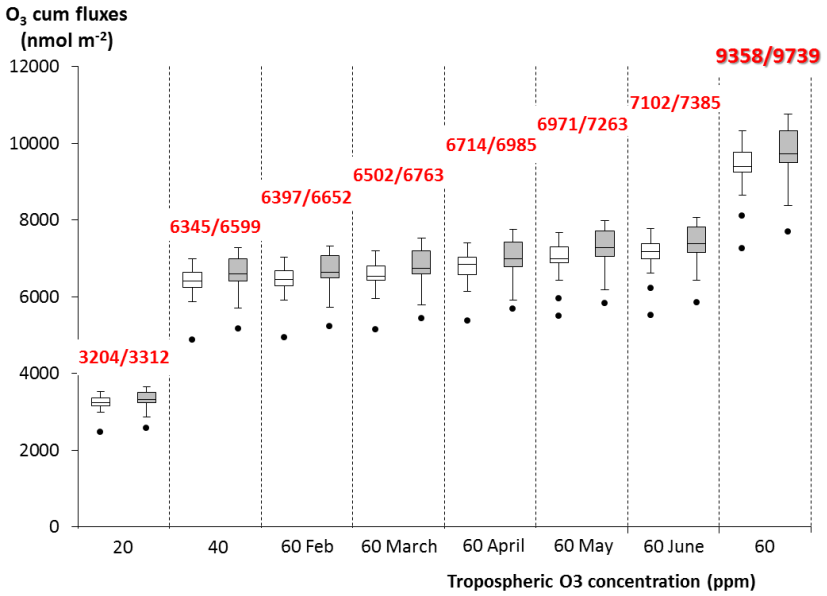

Figure 25. Boxplot of O_3 cum fluxes (nmol m^{-2}) simulated for the pre-industrial, back ground and high ozone concentrations scenarios. Each box is derived from the 19 values simulated for wheat crop in Bremen, Germany. Open boxes refer to rainfed conditions, grey boxes to fully irrigated conditions.

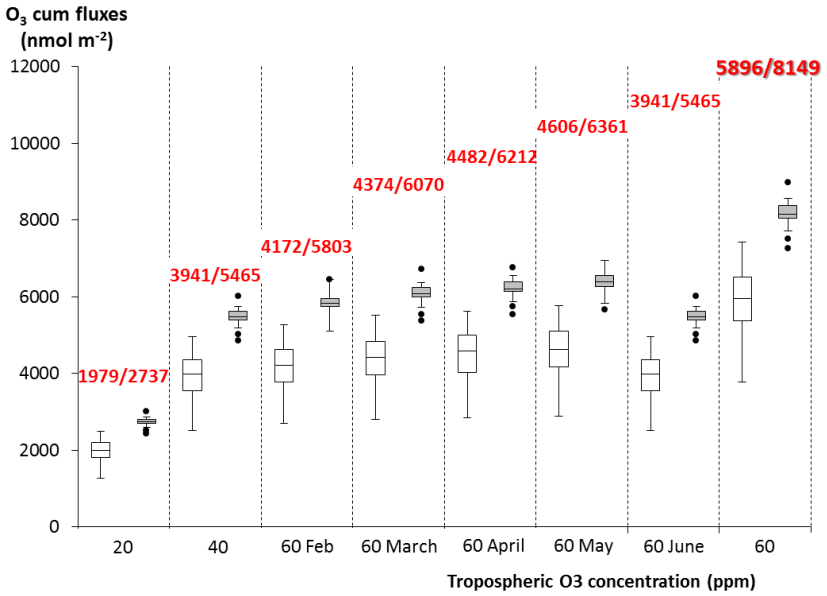

Figure 37. Boxplot of O_3 cum fluxes (nmol m^{-2}) simulated for the pre-industrial, back ground and high Ozone concentrations scenarios. Each box is derived from the 19 values simulated for wheat crop in Jerez de la Frontera, Spain. Open boxes refer to rainfed conditions, grey boxes to fully irrigated conditions.

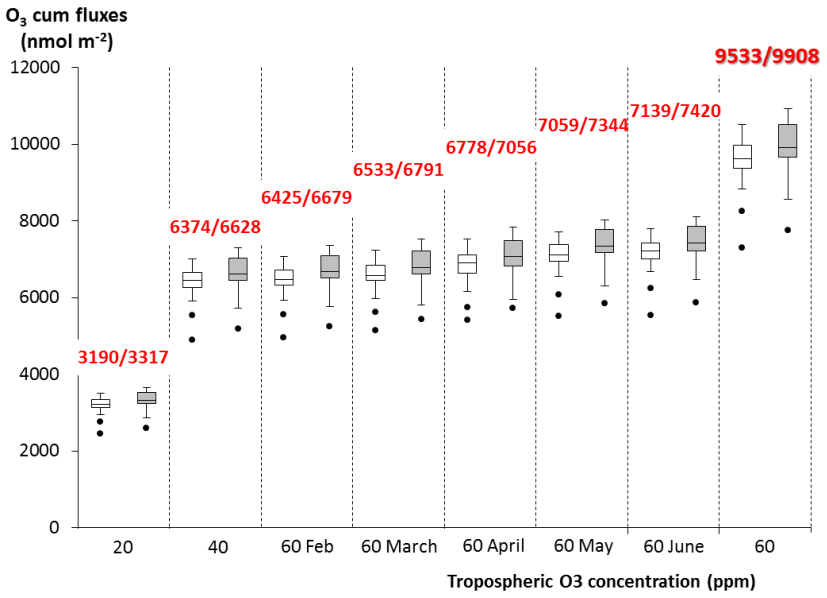

Figure 38. Boxplot of O_3 cum fluxes (nmol m^{-2}) simulated for the pre-industrial, back ground and high Ozone concentrations scenarios. Each box is derived from the 19 values simulated for barley crop in Bremen, Germany. Open boxes refer to rainfed conditions, grey boxes to fully irrigated conditions.

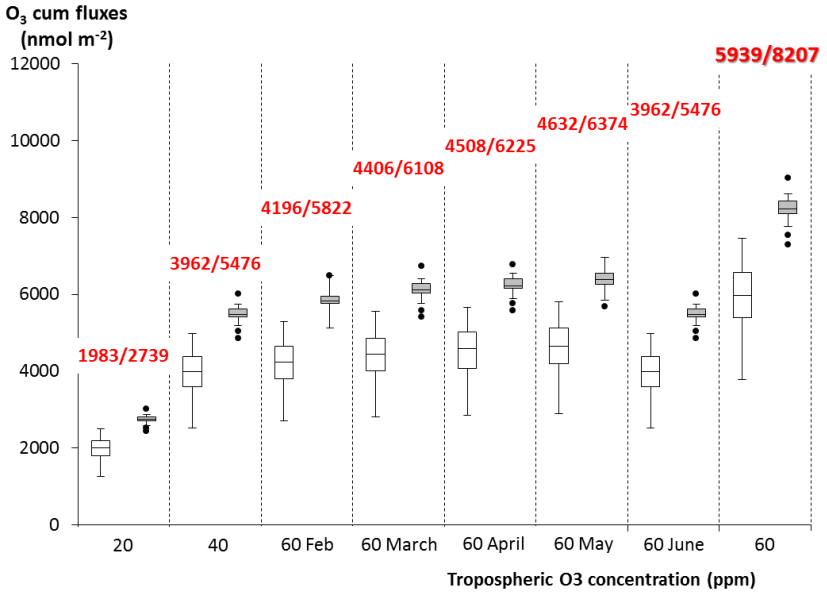

Figure 39. Boxplot of O_3 cum fluxes (nmol m^{-2}) simulated for the pre-industrial, back ground and high Ozone concentrations scenarios. Each box is derived from the 19 values simulated for barley crop in Jerez de la Frontera, Spain. Open boxes refer to rainfed conditions, grey boxes to fully irrigated conditions.

A synthetic overview of the average variability in the 20-years simulated outputs as function of tropospheric O_3 concentration is given in Table 5, where all crop x variety x water management combinations are considered.

Table 5. Comparison of model results concerning crop growth and damage due to ozone exposure under background and high O_3 tropospheric concentrations. The pairs of values refer to rainfed (left) and fully irrigated (right) conditions.

Variable	Bremen		Jerez		unit
	Wheat	*Barley*	*Wheat*	*Barley*	
Tropospheric [O_3] 40 ppb					
Yield*	-7.2;-9.3	-0.4;-0.3	-1.2;-6.4	-0.1;-0.1	%
AGB*	-5.0;-6.4	-0.2;-0.2	-0.7;-3.6	-0.1;-0.1	%
GLAI*	-2.7;-3.0	-0.4;-0.3	-1.4;-1.0	-0.2;-0.3	%
Days O_3flux > [O_3crit]°	64; 73	0.3; 1	14;-61	0; 1	d
Fractional Amax red°	-6.2;-7.2	-0.4;-0.6	-2.1;-7.2	-0.0;-0.6	%
Cumulative O_3 fluxes°	6345; 6599	6374; 6628	3941; 5465	3962; 5476	nmol m^{-2}
Tropospheric [O_3] 60 ppb					
Yield*	-29.4;-32.2	-11.7;-14.4	-11.8;-29.4	-1.3;-11.1	%
AGB*	-22.6;-25.0	-8.7;-10.8	-7.0;-19.3	-0.6;-6.0	%
GLAI*	-11.3;-12.8	-2.5;-3.1	-2.3;-5.4	-0.4;-0.8	%
Days O_3flux > [O_3crit]°	115; 118	74; 83	63;-97	20; 68	d
Fractional Amax red°	-8.8;-20.4	-10.3;-11.4	-10.6;-20.7	-3.8;-11.9	%
Cumulative O_3 fluxes°	9358; 9739	9533; 9908	5896; 8149	6939; 8207	nmol m^{-2}

* percentage difference compared to the pre-industrial scenario; ° absolute values

Based on the above analysis we can make the following general considerations regarding the behavior of the model developed:

1. in general crop damages due to O_3 exposure increase with O_3 concentration.
2. However, the effects of high O_3 concentrations are dependent crop, location, time of exposure simulated variable considered;
3. the highest impact is obtained when the month with high O_3 concentration coincides with the grain filling stage (June for Bremen, April for Jerez);
4. crop damages are more marked in Bremen than Jerez especially under rainfed condition.
5. irrigation practices exacerbate O_3 damages, especially in Jerez;
6. barley is less affected by O_3 impact according to the lower sensitivity of the crop.

6. Conclusions

The WOFOST crop model was extended with algorithms accounting for the effect of ozone on crop growth and yield. The extension encompassed the following elements: a) Effect of water stress on stomatal conductance, b) Ability of plants to recover from ozone damage c) Acceleration of leaf senesce due to O_3 exposure d) Reduction of green leaf area index due to foliar chlorosis or necrosis induced by O_3 e) Reduction of carboxylation rate of Rubisco, f) stomatal slugginesh (not implemented yet). Meteorological datasets with an hourly, and consistent daily resolution were provided for two locations in Germany (Bremen) and Spain (Jerez) encompassing different climatic conditions. To provide synthetic test conditions for the impacts of ozone, the plants were exposed to hypothetical O_3 levels of 20, 40, and 60 ppb during the entire crop growth cycle, and in separate sensitivity tests also for periods of one month to 60 ppb and to 40 ppb for the remainder of the growing season. Two crops where evaluated, wheat which is relatively sensitive to O_3, and barley which is considered to be relatively O_3 insensitive. Two agro-management options were evaluated: fully irrigated (i.e. no water stress) and rain-fed. Irrespective of ozone, wheat and barley yields are lower by only 12 % in Bremen in the absence of irrigation, while reduced by 55 % in Jerez. Wheat yield losses up to 30 % are calculated for ozone concentrations of 60 ppb, and only half of these for barley. Yield losses are substantially smaller in Jerez for rainfed crops, when stomatal closure on the one hand is impeding crop growth and yields, but on the other reducing the impact of ozone. General findings regarding the model behaviour are: a) Crop damages due to O_3 exposure increase with O_3 concentration b) effects of high O_3 concentrations are very heterogeneous depending on month, site, crop and simulated variable considered c) the highest impact is obtained when the month with high O_3 concentration coincides with the maturity period (June for Bremen, April for Jerez) d) crop damage is more marked in Bremen than Jerez and irrigation practice exacerbates O_3 damages, especially in Jerez e) barley is less affected by O_3 impact according to the lower sensitivity of the crop. This behavior corresponds well with general findings in literature reviews on the subject, although only a qualitative comparison is possible on the basis of the *in silico* experiments conducted for this study. Further improvements are possible by:

- extending the model with algorithms to:
    - simulate stomatal sluggishness or disfunctioning, which might be induced at prolonged exposure to high ozone concentration, and
    - simulate the acute reduction of green leaf area index due to foliar chlorosis or necrosis induced by short-term very high doses of O_3.
    - Account for the metabolic costs to plants to avoid (e.g. by producing antioxidants) or repair damage caused by ozone
- The model experiments were performed as sensitivity studies, to learn about model behaviour. Quantitative comparison of model results with real experimental data and with outcomes of more refined models that run with hourly time step.

7. References

Ainsworth, E. A., Yendrek, C. R., Sitch, S., Collins, W. J., Emberson, L. D., 2012. The effects of tropospheric ozone on net primary productivity and implications for climate change. Annual review of plant biology, 63, 637-661.

Allen, R.G., L.S. Pereira, D. Raes, and M. Smith. 1998. Crop evapotranspiration: Guidelines for computing crop water requirements. Irr. & Drain. Paper 56. UN-FAO, Rome, Italy.

Alsher, R.G., Amthor, J.S., 1988. The phyisiology of free-radical scavenging: maintenance and repair processes. In: Schulte Holstede, S. et al. (eds). Air pollution and plant metabolism, Elsevier, London, pp. 94-115.

Amthor, J. S., 1988. Growth and maintenance respiration in leaves of bean (Phaseolus vulgaris L.) exposed to ozone in open-top chambers in the field. New Phytologist, 110(3), 319-325.

Avnery, S., Mauzerall, D. L., Liu, J., Horowitz, L. W., 2011. Global crop yield reductions due to surface ozone exposure: 1. Year 2000 crop production losses and economic damage. Atmospheric Environment, 45(13), 2284-2296.

Biswas, D. K., Xu, H., Li, Y. G., Sun, J. Z., Wang, X. Z., Han, X. G., & Jiang, G. M., 2008. Genotypic differences in leaf biochemical, physiological and growth responses to ozone in 20 winter wheat cultivars released over the past 60 years. Global Change Biology, 14(1), 46-59.

Burney J. and Ramanatan, Recent climate and air pollution impacts on Indian agriculture, PNAS, 2014.

Campbell, G.S., 1985. Soil Physics with BASIC: Transport Models for Soil–Plant Systems. Elsevier, Amsterdam, The Netherlands.

Chen, J.M., Liu, J., Cihlar, J., and M.L. Goulden. 1999. Daily canopy photosynthesis model through temporal and spatial scaling for remote sensing applications. Ecol. Model., 124:99-119.

Confalonieri, R. Inclusion, testing and benchmarking of the impacts of ground-level ozone on yields of selected crops in Europe, Final report, Contract number C392519, 2016.

de Wit, A., Boogaard, H., van Diepen, K., van Kraalingen, D., Rötter, R., Supit, I., Wolf, J., van Ittersum, M., 2015. WOFOST developer's response to article by Stella et al., Environmental Modelling & Software 59 (2014). Environmental Modelling & Software, 73(C), 57-59.

Dentener, F., et al., 2006: The global atmospheric environment for the next generation. Environ. Sci. Technol., 40, 3586–3594.

Diepen, C. V., Wolf, J., Keulen, H. V., & Rappoldt, C., 1989. WOFOST: a simulation model of crop production. Soil use and management, 5(1), 16-24.

Ewert, F., Porter, J.R., 2000. Ozone effects on wheat in relation to CO2: modelling short-term and long-term responses of leaf photosynthesis and leaf duration. Global Change Biology 6, 735-750.

Farquhar G. D. . S. von Caemmerer, J. A. Berry, A biochemical model of photosynthetic CO_2 assimilation in leaves of C_3 species, 1980, Planta 149: 78.

Feng, Z., Kobayashi, K., Ainsworth, E. A., 2008. Impact of elevated ozone concentration on growth, physiology, and yield of wheat (Triticum aestivum L.): a meta-analysis. Global Change Biology, 14, 2696-2708.

Feng, Z., Kobayashi, K., 2009. Assessing the impacts of current and future concentrations of surface ozone on crop yield with meta-analysis. Atmospheric Environment, 43(8), 1510-1519.

Fiore, A.M., Naik, V., Spracklen, D.V., Steiner, A., Unger, N., Prather, M., et al., 2012. Global air quality and climate. Chem. Soc. Rev. 41, 6663–6683.

Forkel, R., Knoche, R., 2006: Regional climate change and its impact on photooxidant concentrations in southern Germany: Simulations with a coupled regional climate-chemistry model. J. Geophys. Res. 111, D12302.

Frère M., and G.F. Popov, Agrometeorological crop monitoring and forecasting, ISBN 9251008078, 1979.

Gamma, E., Helm, R., Johnson, R., Vlissides, J., 1994. Design Patterns: Elements of Reusable Object-Oriented Software. Addison Wesley.

Georgiadis, T., Rossi, S., Nerozzi, F., 1995. Inferring ozone deposition on agricultural surfaces: an application to herbaceous and tree canopies. Water, Air and Soil Pollution 84, 117-128.

Hargreaves, G.H., Samani, Z.A., 1982. Estimating potential evapotranspiration. J. Irrig. and Drain Engr., ASCE 108, 223-230.

Hoshika, Y., Katata, G., Deushi, M., Watanabe, M., Koike, T., Paoletti, E., 2015. Ozone-induced stomatal sluggishness changes carbon and water balance of temperate deciduous forests. Sci Rep 2015 6;5:9871. Epub 2015 May 6.

Kirtman, B., S.B. Power, J.A. Adedoyin, G.J. Boer, R. Bojariu, I. Camilloni, F.J. Doblas-Reyes, A.M. Fiore, M. Kimoto, G.A. Meehl, M. Prather, A. Sarr, C. Schär, R. Sutton, G.J. van Oldenborgh, G. Vecchi and H.J. Wang, 2013: Near-term Climate Change: Projections and Predictability. In: Climate Change 2013: The Physical Science Basis. Contribution of Working Group I to the Fifth Assessment Report of the Intergovernmental Panel on Climate Change [Stocker, T.F., D. Qin, G.-K. Plattner, M. Tignor, S.K. Allen, J. Boschung, A. Nauels, Y. Xia, V. Bex and P.M. Midgley (eds.)]. Cambridge University Press, Cambridge, United Kingdom and New York, NY, USA.

Leuning, R., 1995. A critical appraisal of a combined stomatal-photosynthesis model for C3 plants. Plant, Cell and Environment 18, 339-355.

Medrano, H., Escalona, J.M., Bota, J., Gulìas, J., Flexas, J., 2002. Regulation of photosynthesis of C3 plants in response to progressive drought: stomatal conductance as a reference parameter. Annals of Botany 89, 895-905.

Meteotest 2003. Meteonorm version 5.0. The global meteorological database for engineers, planners and education. Software and data on CD-ROM. James and James, London, United Kingdom.

Mills G, et al. (2007) A synthesis of AOT40-based response functions and critical levels of ozone for agricultural and horticultural crops. *Atmos Environ* 41(12):2630–2643.

Mitchell, G., H. Ray, V.B. Griggs, and J. Williams. 2000. EPIC documentation. Texas A&M Blackland Research and Extension Center, Temple, TX, USA.

Morgan, P. B., Ainsworth, E. A., Long, S. P., 2003. How does elevated ozone impact soybean? A meta-analysis of photosynthesis, growth and yield. Plant, Cell & Environment, 26(8), 1317-1328.

Morgan, P. B., Bernacchi, C. J., Ort, D. R., Long, S. P., 2004. An in vivo analysis of the effect of season-long open-air elevation of ozone to anticipated 2050 levels on photosynthesis in soybean. Plant Physiology, 135(4), 2348-2357.

Pang, J., Kobayashi, K., & Zhu, J., 2009. Yield and photosynthetic characteristics of flag leaves in Chinese rice (Oryza sativa L.) varieties subjected to free-air release of ozone. Agriculture, ecosystems & environment, 132(3), 203-211.

Paoletti, E., Grulke N.E., 2005. Does living in elevated CO2 ameliorate tree response to ozone? A review on stomatal responses. Environmental Pollution 137, 483e493.

Peel, M.C., Finlayson, B.L., McMahon, T. A., 2007. Updated world map of the Köppen–Geiger climate classification. Hydrol. Earth Syst. Sci. 11, 1633–1644.

Pell, E.J., Schlangnhaufer, C.D., Arteca, R.N., 1997. Ozone-induced oxidative stress: Mechanism of action and reaction. Physiologia Plantarum 100, 264-273.

Raes, D., Steduto, P., Hsiao, T.C., Fereres, E., 2009. AquaCrop—The FAO Crop Model to Simulate Yield Response to Water: II. Main Algorithms and Software Description. Agronomy Journal 101, 438-447.

Ritchie, J. T., 1998. Soil water balance and plant water stress. In Understanding options for agricultural production (pp. 41-54). Springer Netherlands.

Semenov, M.A., Barrow, E.M., 2002. LARS-WG. A Stochastic Weather Generator for Use in Climate Impact Studies. User Manual. Rothamsted Research, Harpenden, Hertfordshire AL5 2JQ, UK, 27 p.

Sitch, S., Cox, P.M., Collins, W.J., Huntigford, C., 2007. Indirect radiative forcing of climate change through ozone effects on the land-carbon sink. Nature, 448, 791-795.

Spiker, E.C., Hosker, R.P., Comer, V.J., White, J.R., Werre Jr., R.W., Harmon, F.L., Gandy, G.D., Sherwood S.I., 1992. Environmental chamber for study of the deposition flux of gaseous pollutants to material surfaces. Atmospheric Environment 26, 2885-2892.

Stella, T., Frasso, N., Negrini, G., Bregaglio, S., Cappelli, G., Acutis, M., Confalonieri, R. (2014). Model simplification and development via reuse, sensitivity analysis and composition: a case study in crop modelling. Environmental Modelling & Software, 59, 44-58.

Stevenson, D., R. Doherty, M., Sanderson, C., Johnson, B., Collins, Derwent, D., 2005: Impacts of climate change and variability on tropospheric ozone and its precursors. Faraday Discuss., 130, 41–57.

Tai Amos P. K, M. Val Martin and C.L. Heald Threat to future global food security from climate change and ozone air pollution. *NATURE CLIMATE CHANGE*, 2014

Tian et al., Climate extremes and ozone pollution: a growing threat to China's food security Ecosystem Health and Sustainability, 2, 1-9, 2016. DOI: 10.1002/ehs2.1203

Tuzet, A., Perrier, A., Leuning, R., 2003. A coupled model of stomatal conductance, photosynthesis and transpiration. Plant, Cell and Environment 26, 1097-1116.

Unger, N., D. T. Shindell, D. M. Koch, M. Amann, J. Cofala, and D. G. Streets, 2006: Influences of man-made emissions and climate changes on tropospheric ozone, methane, and sulfate at 2030 from a broad range of possible futures. J. Geophys. Res. Atmos., D12313 111.

Van Dingenen, R., F.J. Dentener, F. Raes, M.C. Krol, L. Emberson, J.Cofal The global impact of ozone on agricultural crop yields under current and future air quality legislation, *Atmos. Env*, 43 (3), p. 605-618, 2009.

Van Ittersum, M.K., P.A. Leffelaar, H.V. Keulen, M.J. Kropff, L. Bastiaans and J. Goudriaan. 2003. On approaches and applications of the Wageningen crop models. European Journal of Agronomy 18: 201-234.

Waichler, S.R., Wigmosta, M.S., 2003. Development of Hourly Meteorological Values From Daily Data and Significance to Hydrological Modelling at H. J. Andrews Experimental Forest. Journal of Hydrometeorology 4, 251-263.

Wild, O., Fiore, A.M., Shindell, D.T., Doherty, R.M., Collins, W.C., Dentener, F.J., et al., 2012: Modelling future changes in surface ozone: A parameterized approach. Atmos. Chem. Phys., 12, 2037-2054.

Wilkinson, S., Davies, W. J., 2009. Ozone suppresses soil drying-and abscisic acid (ABA)-induced stomatal closure via an ethylene-dependent mechanism. Plant, Cell & Environment, 32(8), 949-959.

Williams, J. R., Jones, C.A., Kiniry, J.R., Spaniel, D.A., 1989. The EPIC crop growth model. Transactions of the ASAE, 32(2), 497-511.

8. APPENDICES

APPENDIX A. Patterns of meteorological variables in Jerez de la Frontera and Bremen

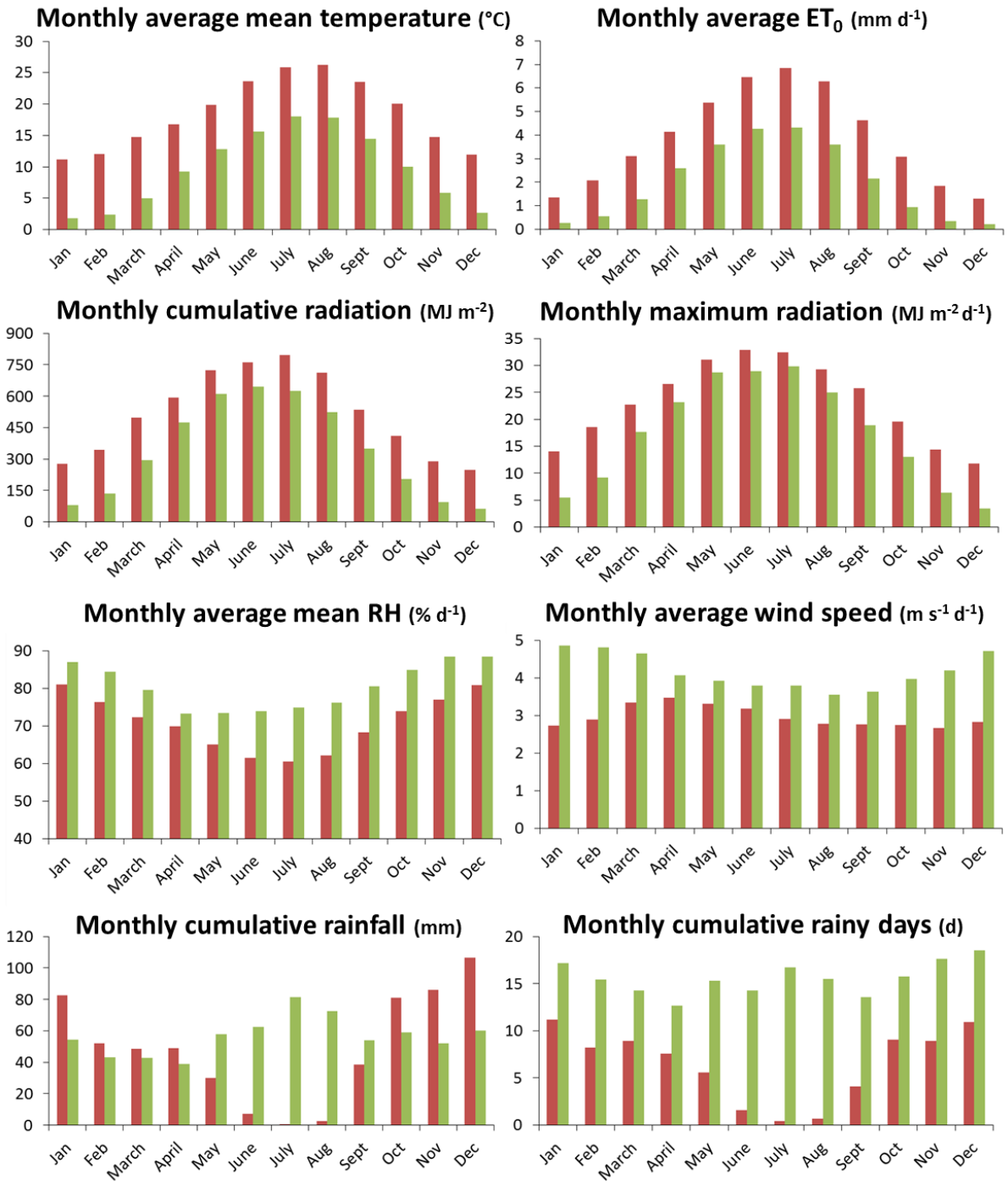

Figure A1 Monthly average values of the meteorological variables recorded by the stations located in Jerez de la Frontera (red bars) and Bremen (green bars) in the period 1996-2015

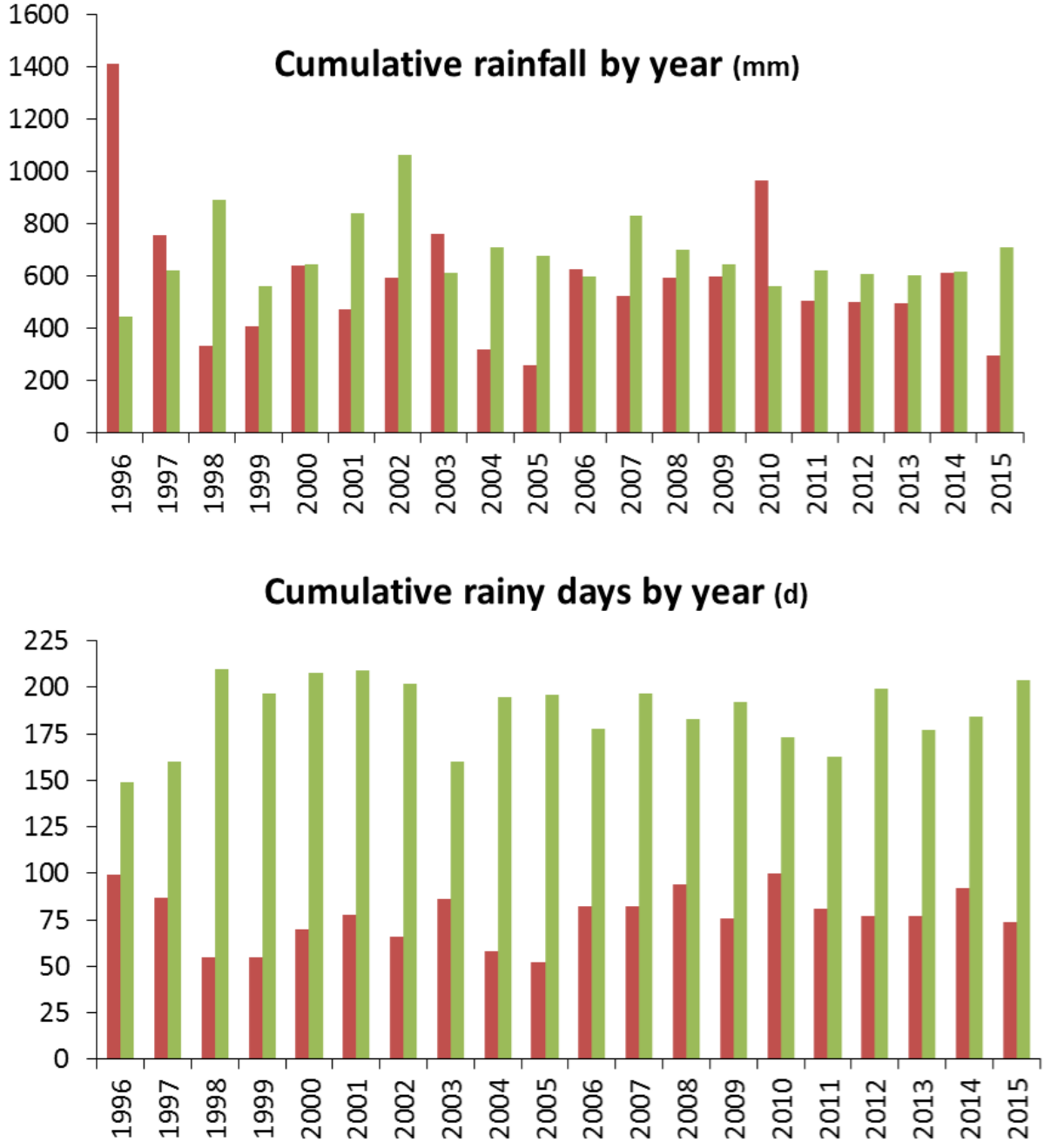

Figure A2. Seasonal values of cumulative rainfall and cumulative rainy days recorded by the stations located in Jerez de la Frontera (red histograms) and Bremen (green histograms) in the period 1996-2015.

APPENDIX B. Short-term effect metacode

```
  if (field.GreenLeafAreaIndex > 0)
                {
                    EstimateOfAssociatedClasses(ozone, impact, weather, field);

                    ozone.O3FluxToStomata = Math.Max((ozone.O3FluxToStomata *
                        ozone.WaterStressCoefficientStomata - PlantSpecificThreshold), 0);
                    ozone.O3FluxToStomata *= hours_O3Uptake;

                    _shorttermo3effect.Estimate(ozone, impact, weather, field);



                }
 foreach (GAIage GAI in field.LeafAreaIndexAge)
                {
                    double recoveryFromO3Damage_Fla = 1;
                    if (GAI.PhysiologicAge_FYSDEL > 0)
                    {
                        recoveryFromO3Damage_Fla = 1 - GAI.PhysiologicAge_FYSDEL / GAI.SPAN;
                    }

                    double incompleteRecovery_RO3s = GAI.ShortTermPhotosinthesis_O3 +
                        (1 - GAI.ShortTermPhotosinthesis_O3) * recoveryFromO3Damage_Fla;

                    double hourlyDecreaseAssimilation_FO3h = 1;
                    if (ozone.O3FluxToStomata > Gamma1/Gamma2 && ozone.O3FluxToStomata < (1+Gamma1)/Gamma2)
                    {
                        hourlyDecreaseAssimilation_FO3h = Math.Min(1 + Gamma1 - Gamma2 * ozone.O3FluxToStomata, 1);
                    }
                    if (ozone.O3FluxToStomata >= (1+Gamma1)/Gamma2)
                    {
                        hourlyDecreaseAssimilation_FO3h = 0;
                    }

                    GAI.ShortTermPhotosinthesis_O3 = hourlyDecreaseAssimilation_FO3h * incompleteRecovery_RO3s;

                    for (int i = 0; i < hours_O3Uptake; i++)
                    {
                        GAI.ShortTermPhotosinthesis_O3 *= hourlyDecreaseAssimilation_FO3h;
                    }
                }
                double sumShortTermReduction = 0;
                for (int i = 0; i < _runTimeData.CropMLDataType.States1_WOFOST_WaterLim_short.LeafAreaIndexAge.Count; i++)
                {
                    _runTimeData.CropMLDataType.States1_WOFOST_WaterLim_short.LeafAreaIndexAge[i].PhysiologicAge_FYSDEL =
_runTimeData.AbioticDamageDataType.Field_short.LeafAreaIndexAge[i].PhysiologicAge_FYSDEL;
```

```
                    _runTimeData.CropMLDataType.States1_WOFOST_WaterLim_short.LeafAreaIndexAge[i].AdjustedSPAN_O3 =
_runTimeData.AbioticDamageDataType.Field_short.LeafAreaIndexAge[i].AdjustedSPAN_O3;


_runTimeData.CropMLDataType.States1_WOFOST_WaterLim_short.LeafAreaIndexAge[i].ShortTermPhotosinthesis_O3 =
_runTimeData.AbioticDamageDataType.Field_short.LeafAreaIndexAge[i].ShortTermPhotosinthesis_O3;


                    sumShortTermReduction +=
_runTimeData.CropMLDataType.States1_WOFOST_WaterLim_short.LeafAreaIndexAge[i].ShortTermPhotosinthesis_O3;
                }


                double avgShortTermReduction = 1;


                if (_runTimeData.CropMLDataType.States1_WOFOST_WaterLim_short.LeafAreaIndexAge.Count != 0)
                {
                    avgShortTermReduction = Math.Min(sumShortTermReduction /
_runTimeData.CropMLDataType.States1_WOFOST_WaterLim_short.LeafAreaIndexAge.Count, 1);
                }


                _runTimeData.CropMLDataType.StatesExt_WOFOST_WaterLim_short.FractionalReductionOfPlantProduction_O3 =
avgShortTermReduction;
```

APPENDIX C. Long-term effect metacode

```
        if (field.GreenLeafAreaIndex > 0)
                {
                    EstimateOfAssociatedClasses(ozone, impact, weather, field);

                    ozone.O3FluxToStomata = Math.Max((ozone.O3FluxToStomata *
                        ozone.WaterStressCoefficientStomata - PlantSpecificThreshold), 0);
                    ozone.O3FluxToStomata *= hours_O3Uptake;

                    _longtermo3effect.Estimate(ozone, impact, weather, field);
                }

foreach (GAIage GAI in field.LeafAreaIndexAge)
                {
                    double ozoneFactor_fO3l = Math.Max(1 - Gamma3 * GAI.CumulatedUptake_O3, 0);

                    double AdjustedSPAN_yesterday = GAI.AdjustedSPAN_O3;
                    GAI.AdjustedSPAN_O3 = GAI.SPAN * ozoneFactor_fO3l;

                    GAI.PhysiologicAge_FYSDEL += Math.Max((AdjustedSPAN_yesterday - GAI.AdjustedSPAN_O3), 0);

                    double senescencePhase_Tlse = 0.33 * GAI.SPAN;
                    double expansionPhase_Tlep = GAI.SPAN - senescencePhase_Tlse;

                    GAI.LeafSenescenceFactor_O3 = 1;

                    if (GAI.PhysiologicAge_FYSDEL > expansionPhase_Tlep)
                    {
                        GAI.LeafSenescenceFactor_O3 = Math.Max(1 - (GAI.PhysiologicAge_FYSDEL -
expansionPhase_Tlep) /
                            (GAI.SPAN / ozoneFactor_fO3l - expansionPhase_Tlep), 0);
                    }

                    GAI.CumulatedUptake_O3 += ozone.O3FluxToStomata / 1000;

double sumSPANReduction = 0;
                for (int i = 0; i <
_runTimeData.CropMLDataType.States1_WOFOST_WaterLim_long.LeafAreaIndexAge.Count; i++)
                {

_runTimeData.CropMLDataType.States1_WOFOST_WaterLim_long.LeafAreaIndexAge[i].PhysiologicAge_FYSDEL =
_runTimeData.AbioticDamageDataType.Field_long.LeafAreaIndexAge[i].PhysiologicAge_FYSDEL;

_runTimeData.CropMLDataType.States1_WOFOST_WaterLim_long.LeafAreaIndexAge[i].CumulatedUptake_O3 =
_runTimeData.AbioticDamageDataType.Field_long.LeafAreaIndexAge[i].CumulatedUptake_O3;

_runTimeData.CropMLDataType.States1_WOFOST_WaterLim_long.LeafAreaIndexAge[i].AdjustedSPAN_O3 =
_runTimeData.AbioticDamageDataType.Field_long.LeafAreaIndexAge[i].AdjustedSPAN_O3;

_runTimeData.CropMLDataType.States1_WOFOST_WaterLim_long.LeafAreaIndexAge[i].LeafSenescenceFactor_O3 =
_runTimeData.AbioticDamageDataType.Field_long.LeafAreaIndexAge[i].LeafSenescenceFactor_O3;
```

```
                    sumSPANReduction +=
_runTimeData.CropMLDataType.States1_WOFOST_WaterLim_long.LeafAreaIndexAge[i].AdjustedSPAN_O3 /
Wofost.LifeSpanOfLeavesGrowingAt35Celsius_SPAN;
                }


                double avgSPANReduction = 1;

                if (_runTimeData.CropMLDataType.States1_WOFOST_WaterLim_long.LeafAreaIndexAge.Count != 0)
                {
                    avgSPANReduction = Math.Min(sumSPANReduction /
_runTimeData.CropMLDataType.States1_WOFOST_WaterLim_long.LeafAreaIndexAge.Count, 1);
                }
                _runTimeData.CropMLDataType.StatesExt_WOFOST_WaterLim_long.FractionalReductionOfSPAN_O3 =
avgSPANReduction;
                }
```

Europe Direct is a service to help you find answers to your questions about the European Union.

Freephone number (*):

00 800 6 7 8 9 10 11

(*) The information given is free, as are most calls (though some operators, phone boxes or hotels may charge you).

More information on the European Union is available on the internet (http://europa.eu).

HOW TO OBTAIN EU PUBLICATIONS

Free publications:

- one copy:
  via EU Bookshop (http://bookshop.europa.eu);
- more than one copy or posters/maps:
  from the European Union's representations (http://ec.europa.eu/represent_en.htm);
  from the delegations in non-EU countries (http://eeas.europa.eu/delegations/index_en.htm);
  by contacting the Europe Direct service (http://europa.eu/europedirect/index_en.htm) or
  calling 00 800 6 7 8 9 10 11 (freephone number from anywhere in the EU) (*).

  (*) The information given is free, as are most calls (though some operators, phone boxes or hotels may charge you).

Priced publications:

- via EU Bookshop (http://bookshop.europa.eu).

LB-NA-28395-EN-N

JRC Mission

As the science and knowledge service of the European Commission, the Joint Research Centre's mission is to support EU policies with independent evidence throughout the whole policy cycle.

EU Science Hub
ec.europa.eu/jrc

@EU_ScienceHub

EU Science Hub - Joint Research Centre

Joint Research Centre

EU Science Hub

Publications Office

doi:10.2788/68501

ISBN 978-92-79-64945-5